

Louisiana State University

LSU Scholarly Repository

LSU Historical Dissertations and Theses

Graduate School

1989

Non-Newtonian Fluid Flow in Eccentric Annuli and Its Application to Petroleum Engineering Problems.

Mustafa Hacıislamoglu

Louisiana State University and Agricultural & Mechanical College

Follow this and additional works at: https://repository.lsu.edu/gradschool_disstheses

Recommended Citation

Hacıislamoglu, Mustafa, "Non-Newtonian Fluid Flow in Eccentric Annuli and Its Application to Petroleum Engineering Problems." (1989). *LSU Historical Dissertations and Theses*. 4848.

https://repository.lsu.edu/gradschool_disstheses/4848

This Dissertation is brought to you for free and open access by the Graduate School at LSU Scholarly Repository. It has been accepted for inclusion in LSU Historical Dissertations and Theses by an authorized administrator of LSU Scholarly Repository. For more information, please contact gradetd@lsu.edu.

INFORMATION TO USERS

The most advanced technology has been used to photograph and reproduce this manuscript from the microfilm master. UMI films the text directly from the original or copy submitted. Thus, some thesis and dissertation copies are in typewriter face, while others may be from any type of computer printer.

The quality of this reproduction is dependent upon the quality of the copy submitted. Broken or indistinct print, colored or poor quality illustrations and photographs, print bleedthrough, substandard margins, and improper alignment can adversely affect reproduction.

In the unlikely event that the author did not send UMI a complete manuscript and there are missing pages, these will be noted. Also, if unauthorized copyright material had to be removed, a note will indicate the deletion.

Oversize materials (e.g., maps, drawings, charts) are reproduced by sectioning the original, beginning at the upper left-hand corner and continuing from left to right in equal sections with small overlaps. Each original is also photographed in one exposure and is included in reduced form at the back of the book.

Photographs included in the original manuscript have been reproduced xerographically in this copy. Higher quality 6" x 9" black and white photographic prints are available for any photographs or illustrations appearing in this copy for an additional charge. Contact UMI directly to order.

U·M·I

University Microfilms International
A Bell & Howell Information Company
300 North Zeeb Road, Ann Arbor, MI 48106-1346 USA
313/761-4700 800/521-0600

Order Number 9025309

**Non-Newtonian fluid flow in eccentric annuli and its application
to petroleum engineering problems**

Haciislamoglu Mustafa, Ph.D.

The Louisiana State University and Agricultural and Mechanical Col., 1989

Copyright ©1990 by Haciislamoglu Mustafa. All rights reserved.

U·M·I

300 N. Zeeb Rd.
Ann Arbor, MI 48106

**NON-NEWTONIAN FLUID FLOW IN ECCENTRIC ANNULI
AND ITS APPLICATION TO PETROLEUM ENGINEERING PROBLEMS**

A Dissertation

**Submitted to the Graduate Faculty of the
Louisiana State University and
Agricultural and Mechanical College
in partial fulfillment of the
requirements for the degree of
Doctor of Philosophy**

in

The Department of Petroleum Engineering

by

**Mustafa Hacıislamoglu
B.S., Istanbul Technical University, 1982
M.S., Louisiana State University, 1985
December 1989**

ACKNOWLEDGEMENT

I wish to thank my major professor, Dr. Julius P. Langlinais, for his encouragement and suggestions throughout this research and for his great help in all aspects of my graduate studies since the very first day I arrived at LSU. I would also like to thank Dr. Lawrence J. Rouse, Jr. for his help and teaching in my minor study. A special appreciation is extended to Petroleum Engineering professors of my examining committee, Dr. Adam T. Bourgoyne, Jr., Dr. Robert Desbrandes, and Dr. Andrew K. Wojtanowicz. I also thank Dr. D. W. Yannitell for his excellent proof reading of this work and serving on the examining committee.

I would like to thank the Department of Education of Turkey and Petroleum Engineering Department at Louisiana State University for providing financial support.

This dissertation is dedicated to my parents and to Sophie.

TABLE OF CONTENTS

	<u>Page</u>
ACKNOWLEDGEMENT.....	ii
LIST OF TABLES.....	v
LIST OF FIGURES.....	vi
ABSTRACT.....	ix
CHAPTER I INTRODUCTION.....	1
CHAPTER II LITERATURE REVIEW.....	6
CHAPTER III MATHEMATICAL MODEL.....	16
3.1 Derivation of the Equation of Motion.....	16
3.2 Bipolar Coordinate System.....	20
3.3 Transformation of the Equation of Motion to Bipolar Coordinates.....	22
3.4 Rheological Model.....	22
3.4.1 The Yield-Power Law Model.....	24
3.5 Dimensional Analysis.....	27
CHAPTER IV NUMERICAL MODEL.....	30
4.1 Discretization of the Equation of Motion	32
4.2 The Boundary Conditions.....	36
4.3 Solution of the Discretized Equation.....	38
CHAPTER V RESULTS.....	43
5.1 Model Verification.....	43
5.2 Velocity Profiles.....	46

	<u>Page</u>
5.3 Viscosity Profiles.....	51
5.4 Frictional Pressure Losses.....	60
5.4.1 A Correlation of Frictional Pressure Loss.....	61
CHAPTER VI APPLICATIONS.....	69
6.1 Surge Pressure Calculations.....	69
6.1.1 Velocity Profiles and Frictional Pressure Loss Calculations with Inner Pipe Motion.....	71
6.1.2 An Example Calculation.....	75
6.2 Displacement of a Gas Kick in Solution in an Oil-Base Mud.....	76
6.2.1 An Example Case.....	78
CHAPTER VII CONCLUSIONS AND RECOMMENDATIONS.....	83
7.1 Conclusions.....	83
7.2 Recommendations.....	85
REFERENCES.....	86
APPENDIX A TRANSFORMATION OF THE EQUATION OF MOTION TO BIPOLAR COORDINATES.....	91
APPENDIX B DERIVATION OF THE DIMENSIONLESS EQUATION OF MOTION.....	94
APPENDIX C FORTRAN LISTING OF THE ECCENTRIC ANNULAR FLOW MODEL.....	97
VITA.....	102

LIST OF TABLES

	<u>Page</u>
2.1 A summary of the literature review.....	15
5.1 Fluid properties and geometry of eccentric annuli.....	46
5.2 Frictional pressure loss gradient data.....	60
6.1 Frictional pressure loss gradient data of the Bingham plastic fluid with inner pipe motion.....	74

LIST OF FIGURES

	<u>Page</u>
1.1 Position of a pipe string in an oil well.....	2
1.2 Position of a pipe string in: (a) concentric annulus (b) eccentric annulus.....	3
1.3 Eccentric annular geometry.....	4
2.1 Representing the concentric annulus as a slot: (a) annular, (b) equivalent slot.....	7
2.2 Representing the eccentric annulus as a slot: (a) annular, (b) equivalent slot.....	9
2.3 The equation of motion in: (a) concentric annulus (b) eccentric annulus.....	10
3.1 The forces acting on a fluid element.....	17
3.2 Bipolar coordinate system.....	20
3.3 Eccentric annulus in bipolar coordinates.....	21
3.4 Rheological models and the flow behavior of drilling fluids and cement slurries.....	23
4.1 Eccentric annulus in: (a) bipolar coordinates, (b) transformed coordinates.....	31
4.2 Grid-point cluster.....	33
4.3 Piecewise-linear profile.....	34
4.4 The grid network.....	37
4.5 Line-by-line method.....	40
5.1 Model verification with CMC solution.....	44

	<u>Page</u>
5.2 Model verification with HEC solution.....	45
5.3 Distribution of grid points in bipolar coordinates:	
(a) uniform, (b) non-uniform.....	47
5.4 The Yield-Power law fluid in concentric annulus, $e=0$::	
(a) 3-D velocity profile, (b) 2-D velocity profile.....	49
5.5 The Yield-Power law fluid in eccentric annulus, $e=0.25$:	
(a) 3-D velocity profile, (b) 2-D velocity profile.....	50
5.6 The Yield-Power law fluid in eccentric annulus, $e=0.5$:	
(a) 3-D velocity profile, (b) 2-D velocity profile.....	52
5.7 The Yield-Power law fluid in eccentric annulus, $e=0.75$:	
(a) 3-D velocity profile, (b) 2-D velocity profile.....	53
5.8 The Bingham plastic fluid in concentric annulus, $e=0$::	
(a) 3-D velocity profile, (b) 2-D velocity profile.....	55
5.9 The Bingham plastic fluid in eccentric annulus, $e=0.4$:	
(a) 3-D velocity profile, (b) 2-D velocity profile.....	56
5.10 Viscosity profile of the Bingham plastic fluid in concentric annulus.....	57
5.11 A schematic of where fluid flows on shear curve.....	58
5.12 Viscosity profile of the Bingham plastic fluid in eccentric annulus, $e=0.4$	59
5.13 Reduction in frictional pressure loss gradient in an annulus of pipe ratios of 0.9.....	63
5.14 Reduction in frictional pressure loss gradient in an annulus of pipe ratios of 0.7.....	64

	<u>Page</u>
5.15 Reduction in frictional pressure loss gradient in an annulus of pipe ratios of 0.5.....	65
5.16 Reduction in frictional pressure loss gradient in an annulus of pipe ratios of 0.3.....	66
5.17 Correlation accuracy.....	67
6.1 Velocity profile in an eccentric annulus while inner pipe is running into hole.....	71
6.2 Velocity profile while inner pipe is moving at 0.5 ft/s: (a) concentric annulus, $e=0.$, (b) eccentric annulus, $e=0.4$	72
6.3 Velocity profile while inner pipe is moving at 1.0 ft/s: (a) concentric annulus, $e=0.$, (b) eccentric annulus, $e=0.4$	73
6.4 A schematic of kick profiling.....	78
6.5 Kick profile in concentric annulus, $e=0$	79
6.6 Flow rate of contaminated oil-base mud at the surface, $e=0$	80
6.7 Kick profile in eccentric annulus, $e=0.5$	81
6.8 Flow rate of contaminated oil-base mud at the surface, $e=0.5$	82

ABSTRACT

The fluid flow in the annular gap in oilwells is a complex problem. The geometry of the annulus is customarily simplified to concentric annular flow. In this study, a fluid flow model is developed allowing annulus to be eccentric: inner pipe located anywhere in the annulus. Thus, a more realistic representation of the actual geometry is obtained.

An equation of motion that defines flow of non-Newtonian fluids in eccentric annuli is derived. A numerical solution of this equation is presented. The velocity profiles, the viscosity profiles, and the flow rate vs frictional pressure loss gradient relationship are calculated for varying eccentricities. The velocity profiles, and the viscosity profiles are compared to widely used substitutes: the average velocity and the apparent viscosity, respectively. A correlation based on the model generated data is developed that permits for an easy calculation of the frictional pressure losses in eccentric annuli.

Generally neglected eccentricity is introduced to two problems of petroleum engineering: surge pressure calculations and displacement of a gas kick in solution in an oil-base mud. The results are found to be a strong function of eccentricity.

CHAPTER I

INTRODUCTION

A common assumption for annular flow used in the petroleum industry is that the inner pipe is concentrically located inside the flow geometry; however, this is rarely the case, even in slightly deviated wells. For example, in a 12.25 in. diameter hole with only one degree of deviation from vertical, a 4.5 in. OD drillpipe will become fully eccentric (drillpipe touching the borehole) before it reaches the depth of 20 ft. Since it is impossible in conventional drilling to keep the inclination of a hole perfectly vertical, the position of pipe in the hole will invariably change and be eccentric. Figure 1.1 shows a possible positioning of a drillpipe in an oil well and suggests that any fluid flow in the annular space between the pipe and the hole is a 3-dimensional problem. This 3-D problem is extremely difficult to solve because:

- a. the exact location of inner pipe as a function of depth can not be determined.
- b. the equations that define fluid flow in such a geometry are very complex, and consequently their solution is rather lengthy.

Therefore, annular flow in oil wells is traditionally reduced to a 1-D problem assuming a concentric annulus (Fig. 1.2a):

- a. the position of the pipe is not a function of depth.
- b. the pipe is always centered in the annulus.

In this case, The equation of motion is quite simple and with a slot flow approximation of the annular geometry (explained in Chapter II), an analytical solution to the problem can be obtained.

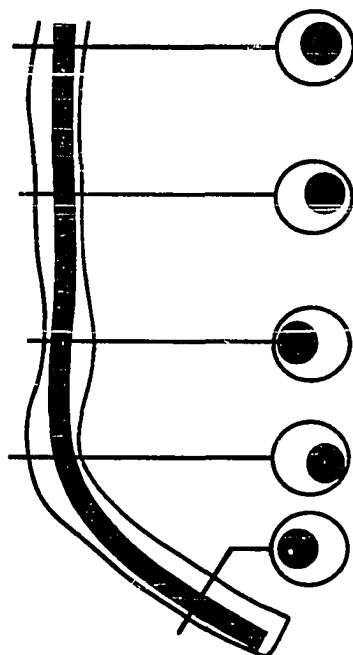


Fig. 1.1 Position of a pipe string in an oil well

A less idealistic approach may be obtained by removing the second assumption of 1-D case. If the inner pipe is allowed to be anywhere in the annulus, the problem is then 2-D (Fig. 1.2b), and

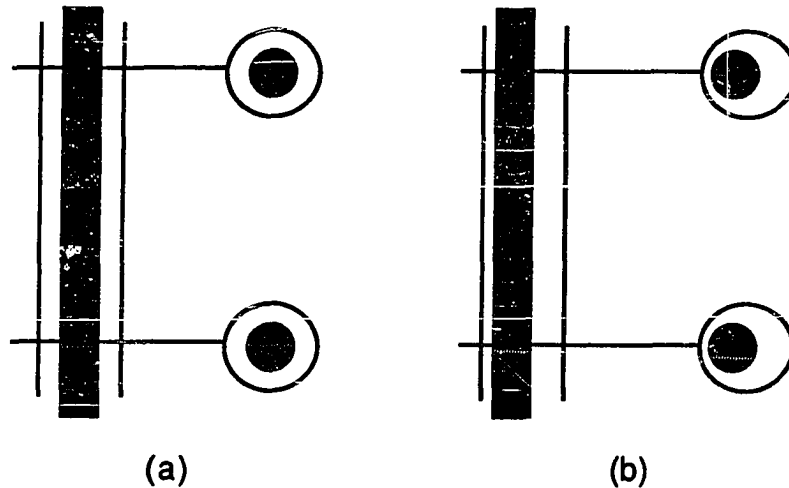


Fig. 1.2 Position of a pipe string in: (a) concentric annulus
(b) eccentric annulus

the equation of motion in this case can be solved numerically. This solution may be quite realistic in directional and horizontal wells. Considering the increasing number of such wells, the flow behavior of drilling fluids and cement slurries in eccentric annulus is gaining interest. This 2-D problem of fluid flow in an annulus will be investigated in this study. The location of the inner pipe in the annular space will be specified with variable eccentricity. Before further discussion, one must define eccentricity.

Eccentricity is defined as a dimensionless number, e , which is equal to zero for a concentric annulus and is equal to one for a fully eccentric annulus. A schematic of an eccentric annulus is shown in Fig. 1.3. The eccentricity is given by

$$e = \frac{2\delta}{d_o - d_i} \quad (1.1)$$

where e = eccentricity, dimensionless
 δ = distance between the centers of inner and outer pipes, L
 d_o = outer pipe diameter, L
 d_i = inner pipe diameter, L

In directional drilling or cementing operations where the inner pipe coupling or centralizer is assumed to be touching the outer pipe or borehole, the eccentricity is calculated as

$$e = \frac{d_o - d_c}{d_o - d_i} \quad (1.2)$$

where d_c = diameter of coupling or centralizer, L

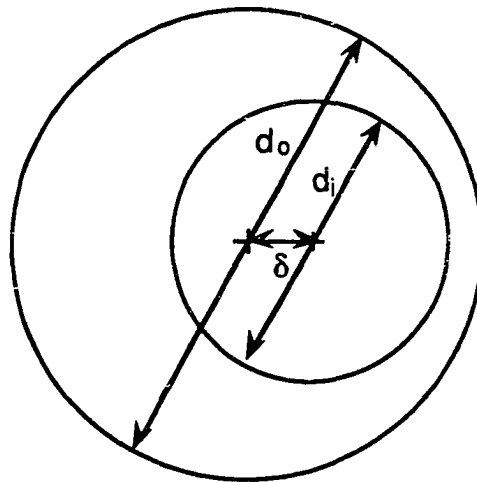


Fig. 1.3 Eccentric annular geometry

In many areas of petroleum engineering, accurate predictions of velocity, viscosity profiles, and frictional pressure loss gradients across the annulus are needed. Accounting for eccentricity will enhance the accuracy of numerous mathematical models used in drilling hydraulics since many of these models depend heavily upon the velocity profile and the frictional pressure losses in the annulus. Such problems as cuttings transport, surge pressure calculations, displacement of kicks from the bottom of the hole to the surface, and mud displacement in cementing operations, etc. are all dependent on a satisfactory description of annular flow.

CHAPTER II

LITERATURE REVIEW

Lamb (1932) was the first to derive an equation that related flow rate and frictional pressure drop for laminar, steady-state flow of Newtonian fluids in a concentric annulus. Lamb's equation is:

$$Q = \frac{\pi}{8\mu} \frac{\Delta P_f}{\Delta L} \left[r_o^4 - r_i^4 - \frac{(r_o^2 - r_i^2)^2}{\ln S} \right] \quad (2.1)$$

where Q = flow rate, $L^3 T^{-1}$

μ = viscosity, $M L^{-1} T^{-1}$

$\frac{\Delta P_f}{\Delta L}$ = frictional pressure loss gradient, $M L^{-2} T^{-2}$

r_o = radius of inner pipe, L

r_i = radius of outer pipe, L

S = pipe radius ratio, r_i/r_o , dimensionless

Fredrickson and Bird (1958), in their well-known study, analyzed non-Newtonian fluids, namely, Bingham plastic and Power law in concentric annulus. The relationship between flow rate and frictional pressure gradient was published in the form of a set of graphs for a complete solution. Also, an analytical solution was derived for a slot flow approximation (Fig. 2.1) for a concentric annulus which is considered to be reasonably accurate

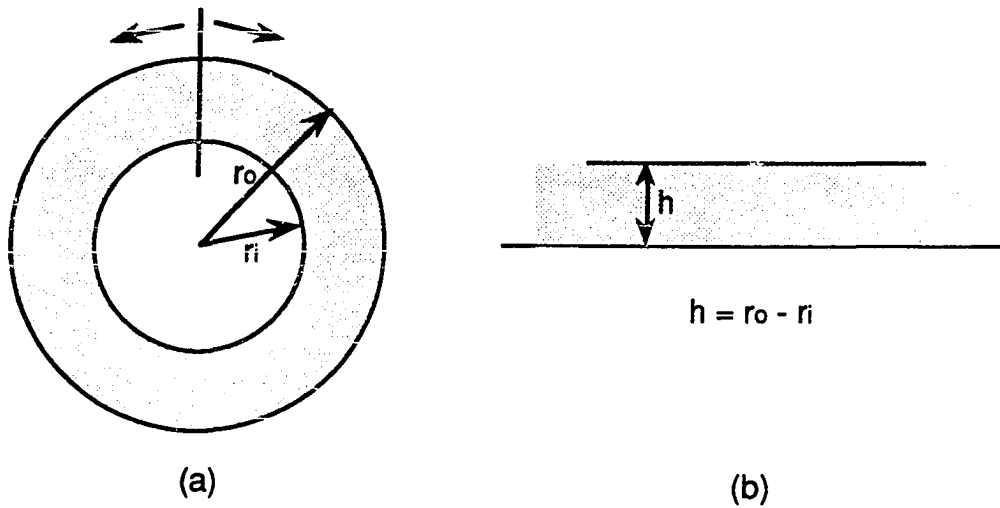


Fig. 2.1 Representing the concentric annulus as a slot:

(a) annular, (b) equivalent slot

for $r_i/r_o > 0.3$ (Bourgoyne, 1986). These equations for Bingham plastic and Power law fluids are, respectively:

$$Q = \frac{\pi r_o^4}{6\mu_p} \frac{\Delta P_f}{\Delta L} (1 - S)^3 \left[1 - \frac{3}{2} \left(\frac{\tau_o}{1 - S} \right) + \frac{1}{2} \left(\frac{\tau_o}{1 - S} \right)^3 \right] \quad (2.2)$$

$$Q = \frac{\pi r_o^3}{\frac{1}{n} + 2} \left(\frac{\Delta P_f}{\Delta L} \frac{r_o}{2K} \right)^{\frac{1}{n}} (1 - S)^{\frac{1}{n} + 2} \quad (2.3)$$

where τ_o = yield point, $M L^{-1} T^{-2}$

μ_p = plastic viscosity, $M L^{-1} T^{-1}$

K = consistency index, $M L^{-1} T^{n-2}$

n = flow behavior index, dimensionless

Later came the eccentric annular flow studies which chose one of the two basic approaches to the problem;

1. approximation of eccentric annular geometry with a narrow slot
2. complete definition of eccentric annular geometry in bipolar coordinates

An early study in this area was done by Tao and Donovan (1955). In this experimental and theoretical work, flow of Newtonian fluids in an eccentric annulus with and without rotation of the inner pipe are addressed. In the theoretical part of the work, several simplifying assumptions are made, some of which led to incorrect flow rate predictions. Tao and Donovan approximated the eccentric annulus with a slot of variable height (Fig. 2.2). The first source of error is the expression used to define the variable slot height, h , given by:

$$h = (r_o - r_i)(1 + e \cos\theta) \quad (2.4)$$

where h = slot height, L

r_o = radius of inner pipe, L

r_i = radius of outer pipe, L

e = eccentricity, dimensionless

θ = eccentricity angle defined in Fig. 2.2, degree

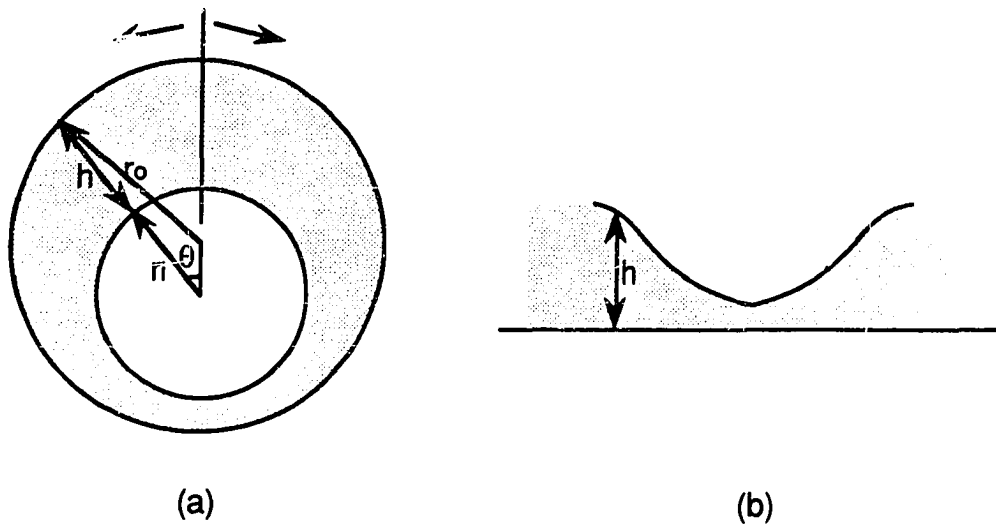


Fig. 2.2 Representing the eccentric annulus as a slot:

(a) annular (b) equivalent slot

The assumption in the above equation is that both the radial clearance, $r_o - r_i$, and the eccentricity, e , are small, limiting its use significantly. The second source of error, even more important, is that the equation of fluid motion used by Tao and Donovan was valid only for concentric annular flow. That is shear stress was assumed to occur in one dimension only. In Cartesian coordinates, it is:

$$\frac{\partial \tau_{yz}}{\partial y} = \frac{\Delta P_f}{\Delta L} \quad (2.5)$$

Figure 2.3 shows the slot flow approach to concentric and eccentric annular flow with the valid equations of motion in each

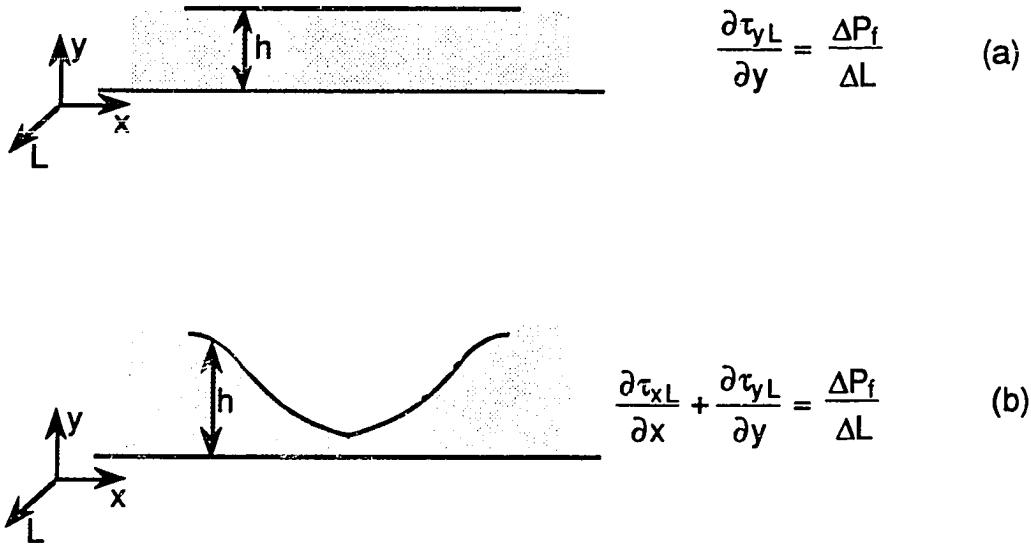


Fig. 2.3 The equation of motion in: (a) concentric annulus
(b) eccentric annulus

case. In other words, Tao and Donovan, like many other researchers to follow, accounted for shear only in the y -direction while ignoring shear in the x -direction that certainly exists in eccentric annular flow.

In 1959, Heyda presented a technique to calculate velocity profiles for Newtonian fluids in eccentric annulus employing the appropriate equation of motion.

$$\frac{\partial \tau_{xz}}{\partial x} + \frac{\partial \tau_{yz}}{\partial y} = \frac{\Delta P_f}{\Delta L} \quad (2.6)$$

Utilizing bipolar coordinates, which is the most suitable coordinate system to represent eccentric annular geometry (see

Chapter III for information on bipolar coordinates), and the Green's function, Heyda obtained the velocity profile in the form of an infinite series. He made no attempt to obtain the corresponding flow rates. Three years later, Redberger and Charles (1962) applied the finite differences technique to solve the differential equation of motion for the velocity profile. This was numerically integrated to arrive at the relationship for flow rate vs frictional pressure loss gradient. Their velocity profile agreed with Heyda's analytical solution. Snyder and Goldstein (1965) also analyzed Newtonian fluid flow in an eccentric annulus using a technique similar to Heyda's. Making use of the velocity profile, they developed expressions for shear stress at the inner and outer pipe walls and related these to friction factor calculations.

In the meantime, Vaughn (1965) was the first to pursue a solution for non-Newtonian (Power law) fluid flow with a slot flow approximation of an eccentric annulus. Unfortunately, his variable slot height equation (Eq. 2.4) and the equation of motion (Eq. 2.5) was the same as Tao and Donovan's. Therefore, he also concluded an erroneous flow rate vs frictional pressure loss gradient relation. In 1973, Mitsuishi and Aoyagi experimented with non-Newtonian solutions in small scale eccentric annuli. They confirmed that the frictional pressure loss in an eccentric annulus decreases as the eccentricity increases for a fixed flow rate. The further evidence of this behavior is also found in experimental studies of turbulent flow of Newtonian fluids in

eccentric annuli (Dodge, 1963; Jonsson and Sparrow, 1966). Dodge ran experiments using pipe diameter ratios of 0.875, 0.750 and 0.688 with eccentricities ranging 0. to 1. in the Reynolds-number range of 20,000 to 100,000. The experimental data show that the frictional pressure loss is reduced as eccentricity increases for a constant Reynolds-number. Jonsson and Sparrow have also used an experimental apparatus to measure frictional pressure losses in the Reynolds-number range of 18,000 to 180,000. The experimental apparatus consisted of an outer pipe of 4.08 in. and inner pipes of 3.004, 2.248 and 1.124 inches. They had measured frictional pressure losses and point velocities. Jonsson and Sparrow reported "for a fixed diameter ratio and Reynolds number, the friction factor decreases with increasing eccentricity." With their laminar flow experiments, Mitsuishi and Aoyagi also observed that increasing non-Newtonian behavior slows the rate of decreasing frictional pressure drop as eccentricity increases.

Guckes (1975) presented one of the better studies in the area. Adopting bipolar coordinates and the finite difference technique, he solved the equation of motion (Eq. 2.6) for eccentric annular flow of a Power law and a Bingham plastic fluid. Velocity profiles are numerically integrated over the annular area to obtain a relationship between flow rate and frictional pressure gradient; however, the computational difficulties and instability of the computer model at high eccentricities limited the range of study.

Six years after Guckes, Iyoho and Azar (1981) presented an analytical solution of Power law fluid flow in an eccentric annulus claiming to avoid Vaughn's simplifying assumptions so that their velocity profiles are comparable in accuracy with the studies done by previous investigators using bipolar coordinates and iterative numerical methods. In fact, they corrected the inaccurate form of the variable slot height used by Tao and Donovan and Vaughn. Iyoho and Azar derived a complete equation for variable slot height

$$h = (r_o^2 - e^2 \cos^2 \theta)^{\frac{1}{2}} - r_i + e \cos \theta \quad (2.7)$$

where $c = r_o - r_i$

However, their equation of motion (Eq. 2.5) was still incorrect resulting in the calculation of unacceptably high velocities, more than 100 % in error in some cases.

Two recent studies by Luo and Peden (1987) and Uner *et al* (1989) also used the slot flow approximation. Uner *et al* adopt an approach similar to Iyoho and Azar's study with some modifications to the equivalent slot calculations while Luo and Peden use a slot with a varying outer radius instead of varying the inner radius. Both studies also employ the equation of motion (Eq. 2.5) for concentric annular flow in eccentric annulus, and therefore result in error.

Primarily, this literature review shows that all analytical solution attempts, approximating an eccentric annulus with an

equivalent slot, have fallen short mainly because they used the incorrect equation of motion (Table 2.1). Unfortunately, when the appropriate equation of motion (Eq. 2.6) is applied to the slot flow approximation of eccentric annular geometry, a closed form mathematical solution does not yield, leaving one choice: a numerical solution. In that case, the bipolar coordinate system is used to exactly define the eccentric annular geometry rather than approximating it with a slot.

The flow of non-Newtonian fluids in eccentric annulus must be investigated for a full range of eccentricities and pipe radius ratios. In this dissertation, a numerical solution of the equation of motion for eccentric annulus in bipolar coordinates with a three-constant rheological model (the Yield-Power law) that matches drilling mud and cement slurry behavior is developed. The flow rate vs frictional pressure gradient relationship is presented and, more importantly, the velocity and the viscosity distributions that provide invaluable insight to all annular flow related drilling engineering problems are discussed.

Table 2.1 A summary of literature

RESEARICHERS	RHEOLOGICAL MODEL	GEOMETRICAL DEFINITION OF ECCENTRIC ANNULUS	EQ. OF MOTION IN ECCENTRIC AN.	TYPE OF SOLUTION	RESULTS
Tao and Donovan 1955	Newtonian	Slot flow approx. Inaccurate slot height	1-D shear	Analitical	incorrect Q vs $\Delta P_f / \Delta L$
Heyda 1959	Newtonian	Bipolar	2-D shear	Analitical	Velocity profile
Redberger and Charles 1962	Newtonian	Bipolar	2-D shear	Numerical	flowrate
Snyder and Goldstein 1965	Newtonian	Bipolar	2-D shear	Analitical	Shear stress and friction factor calc.
Vaughn 1965	Power-law	Slot flow approx. Inaccurate slot height	1-D shear	Analitical	incorrect Q vs $\Delta P_f / \Delta L$
Guckes 1975	Bingham plastic Power-law	Bipolar	2-D shear	Numerical	Q vs $\Delta P_f / \Delta L$ with limited ecc. range
Iyoho and Azar 1980	Power-law	Slot flow approx. Accurate slot height	1-D shear	Analitical	Incorrect velocity profile
Luo and Peden 1987	Bingham plastic Power-law	Slot flow approx. Accurate slot height	1-D shear	Analitical	Incorrect vel. profile and shear stress
Uner and Ozgen Toşun 1989	Power-law	Slot flow approx. Accurate slot height	1-D shear	Analitical	Incorrect flow rate

CHAPTER III

MATHEMATICAL MODEL

3.1 Derivation of the Equation of Motion

This chapter provides an analysis of the steady-state laminar flow of incompressible fluids in an eccentric annulus. For simplicity, a Cartesian coordinate system will be used to develop the governing equation of motion. However, the equation obtained here will be transformed into bipolar coordinates later to help define eccentric annular geometry. Flow is in the L-direction and fully developed; that is, it is not influenced by entrance effects, and the velocity profile does not vary along the axis of flow. Consider a cubical fluid element having dimensions Δx , Δy , and ΔL (Fig. 3.1). By applying Newton's law of motion to the fluid element, a relationship between shear stress, τ , and frictional pressure drop, $\Delta P_f / \Delta L$, is derived. The forces acting on the fluid element are shown in Fig. 3.1. The force F_1 is applied by the fluid pressure and given by:

$$F_1 = \left(P - \frac{\partial P_f}{\partial L} \frac{\Delta L}{2} \right) \Delta x \Delta y \quad (3.1)$$

P is the pressure in the center of the cube, and the sign convention in Fig. 3.1 is being used. Similarly, the force F_2

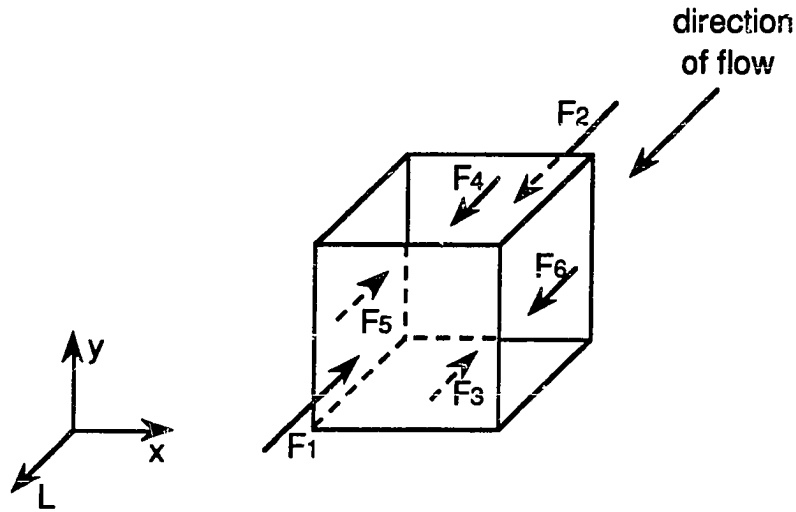


Fig. 3.1 The forces acting on a fluid element

applied by the fluid pressure is given by:

$$F_2 = \left(P + \frac{\partial P_f}{\partial L} \frac{\Delta L}{2} \right) \Delta x \Delta y \quad (3.2)$$

The frictional forces on the sides of the cube exerted by the adjacent fluid elements are

$$F_3 = \left(\tau_{yL} - \frac{\partial \tau_{yL}}{\partial y} \frac{\Delta y}{2} \right) \Delta x \Delta L \quad (3.3)$$

$$F_4 = \left(\tau_{yL} + \frac{\partial \tau_{yL}}{\partial y} \frac{\Delta y}{2} \right) \Delta x \Delta L \quad (3.4)$$

$$F_5 = \left(\tau_{xL} - \frac{\partial \tau_{xL}}{\partial x} \frac{\Delta x}{2} \right) \Delta y \Delta L \quad (3.5)$$

$$F_6 = \left(\tau_{xL} + \frac{\partial \tau_{xL}}{\partial x} \frac{\Delta x}{2} \right) \Delta y \Delta L \quad (3.6)$$

The usual method of identification of shear stress is used in the above equations. The first subscript is the direction of the axis to which the plane of action of shear stress is normal, and the second subscript is the direction of action of shear stress. The sum of the forces acting on the fluid element must equal zero because the flow is in a steady state, and the fluid element is moving at constant velocity in the L-direction.

$$F_1 - F_2 + F_3 - F_4 + F_5 - F_6 = 0 \quad (3.7)$$

When Eqs. 3.1-3.6 are substituted into Eq. 3.7, and simplified, the result is:

$$\frac{\partial P_f}{\partial L} - \frac{\partial \tau_{xL}}{\partial x} - \frac{\partial \tau_{yL}}{\partial y} = 0 \quad (3.8)$$

Shear stresses are defined as (Welty, 1984):

$$\tau_{xL} = -\mu \left(\frac{\partial v_L}{\partial x} + \frac{\partial v_x}{\partial L} \right) \quad (3.9)$$

$$\tau_{yL} = -\mu \left(\frac{\partial v_y}{\partial L} + \frac{\partial v_L}{\partial y} \right) \quad (3.10)$$

Since the flow is in the L-direction only

$$v_x = v_y = 0, \quad v_L \neq 0 \quad (3.11)$$

which simplifies shear stresses to:

$$\tau_{xL} = -\mu \frac{\partial v_L}{\partial x} \quad (3.12)$$

$$\tau_{yL} = -\mu \frac{\partial v_L}{\partial y} \quad (3.13)$$

Equation 3.8 may be written in terms of velocity:

$$\frac{\partial P_f}{\partial L} + \frac{\partial}{\partial x} \left(\mu \frac{\partial v_L}{\partial x} \right) + \frac{\partial}{\partial y} \left(\mu \frac{\partial v_L}{\partial y} \right) = 0 \quad (3.14)$$

Since there is only one non-zero velocity component in Eq. 3.14, the subscript L may be ignored. Also, the frictional pressure loss gradient term will be expressed as $\Delta P_f / \Delta L$ from now on since it is a constant. The general form of the equation of motion in a cartesian coordinate system is, therefore,:

$$\frac{\Delta P_f}{\Delta L} + \frac{\partial}{\partial x} \left(\mu \frac{\partial v}{\partial x} \right) + \frac{\partial}{\partial y} \left(\mu \frac{\partial v}{\partial y} \right) = 0 \quad (3.15)$$

Equation 3.15 is very similar to a simplified version of the Navier-Stokes equation except that the viscosity term here is not taken out of the derivative since it is not necessarily a constant.

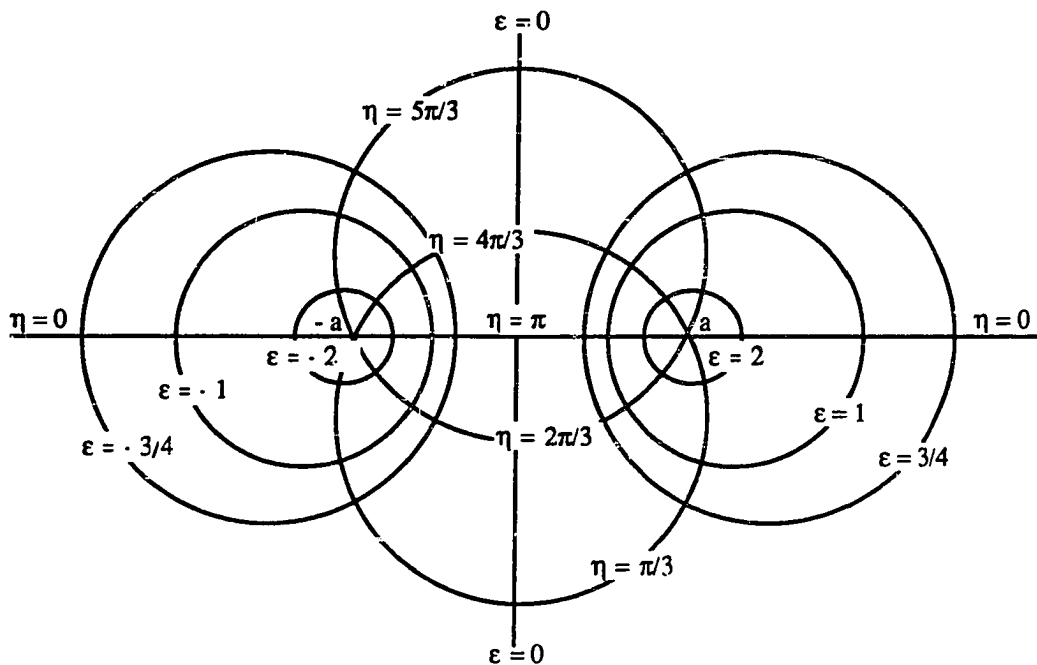


Fig. 3.2 Bipolar coordinate system

3.2 Bipolar Coordinate System

Eccentric annular geometry is best defined in a bipolar coordinate system, which consists of two orthogonal families of circles, ϵ and η (Fig 3.2). The walls of an eccentric annulus are represented by two constant values of ϵ while η , varying from 0 to 2π , scans the eccentric annulus (Fig 3.3). L is the third axis which is perpendicular to ϵ and η . The relationships needed to transform from Cartesian coordinates to bipolar coordinates are given by (Speigel, 1968):

$$x = \frac{a \sinh \epsilon}{\cosh \epsilon - \cos \eta} \quad (3.16)$$

$$\epsilon_o = \cosh^{-1} \left[\frac{(1 + S) - e^2 (1 - S)}{a e} \right] \quad (3.21)$$

where e = eccentricity, dimensionless

S = pipe radius ratio, r_i/r_o , L

3.3 Transformation of the Equation of Motion to Bipolar Coordinates

The equation of motion, Eq. 3.15, in Cartesian coordinates was previously developed. Transformation of the equation to bipolar coordinates allows the eccentric annular geometry to be handled. Details of the transformation are provided in Appendix A, and the final form of the transformed equation of motion in bipolar coordinates is

$$\left(\frac{a}{\psi} \right)^2 \frac{\Delta P_f}{\Delta L} + \frac{\partial}{\partial \epsilon} \left(\mu \frac{\partial v}{\partial \epsilon} \right) + \frac{\partial}{\partial \eta} \left(\mu \frac{\partial v}{\partial \eta} \right) = 0 \quad (3.22)$$

$$\text{where } \psi = \cosh \epsilon - \cos \eta \quad (\epsilon_o \leq \epsilon \leq \epsilon_i, \quad 0 \leq \eta \leq 2\pi) \quad (3.23)$$

The next step is to define μ , where a rheological model is selected.

3.4 Rheological Model

Drilling muds and cement slurries, known to be non-Newtonian fluids, are the two most common groups of fluids that

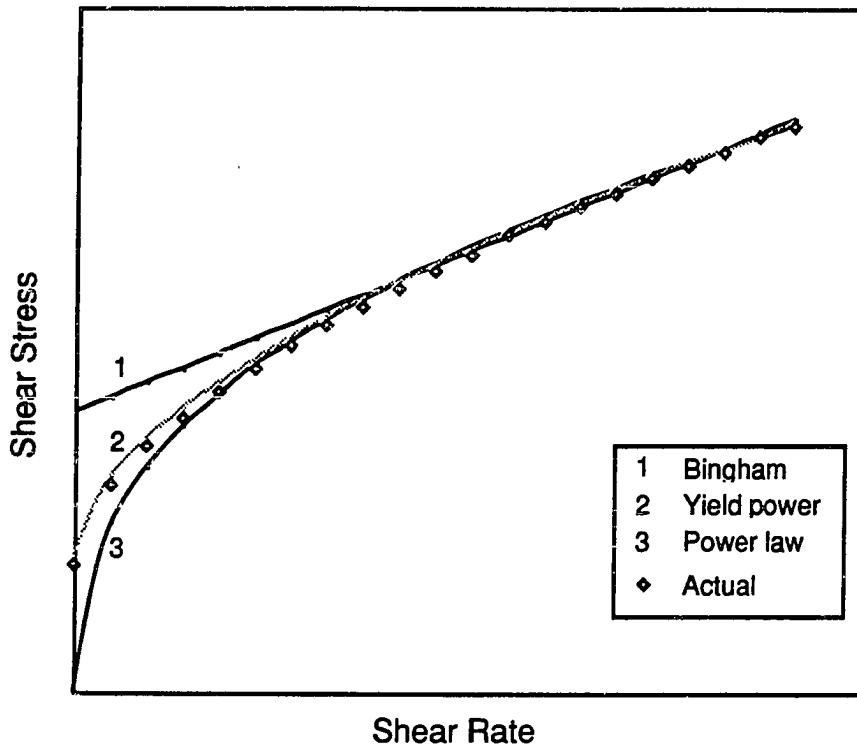


Fig. 3.4 Rheological models and the flow behavior of drilling fluids and the cement slurries

are encountered in annular flow by petroleum engineers. The shear rate vs shear stress relationship of these fluids and the performance of some rheological models in defining the actual flow behavior of these fluids is shown in Fig. 3.4. Bingham plastic and Power law models, widely used in the petroleum industry because of their simplicity, are limited in their ability to define the actual flow behavior of drilling muds and cement slurries. Both drilling muds and cement slurries are pseudo-plastic fluids with a yield point (Denis, 1987; Zamora, 1974) and

display an intermediate behavior when compared to Bingham plastic and Power law models. The Herschel and Bulkley (1926) rheological model, also called the Yield-Power law model, closely matches the flow behavior of the fluids in question; and, therefore, will be used in this study.

3.4.1 The Yield-Power Law Model

The Yield-Power law formulation of shear rate–shear stress relationship is defined as:

$$\tau = \tau_0 + K\dot{\gamma}^n \quad (3.24)$$

where τ = shear stress, $M L^{-1} T^{-2}$

τ_0 = yield point, $M L^{-1} T^{-2}$

K = consistency index, $M L^{-1} T^{n-2}$

n = flow behavior index, dimensionless

$\dot{\gamma}$ = shear rate, T^{-1}

The determination of the model constants, τ_0 , n , and K , for a Yield-Power law fluid is unfortunately not as easy as two constant models such as Bingham plastic and Power law. The exact analytical equations to calculate Yield-Power law model constants directly from a standard rotational viscometer data do not exist unless the yield point of the fluid is known. Then, to calculate n and K , Power law model equations need to be shifted by an amount equal to the zero rpm reading, θ_0 (yield point, τ_0 , in lb/100 ft² is numerically equal to the viscometer dial reading at

zero rpm) (Zamora, 1974):

$$n = 3.322 \log \left(\frac{\theta_{600} - \theta_0}{\theta_{300} - \theta_0} \right) \quad (3.25)$$

$$K = \frac{510 (\theta_{300} - \theta_0)}{511^n} \quad (3.26)$$

where θ_{300} and θ_{600} are the rotational viscometer dial readings at 300 rpm and 600 rpm, respectively. Even though the literature (Zamora, 1974; Imco, 1983) recommends the substitution of zero or 3 rpm dial reading for yield point for such fluids, making measurements at low shear rates with a standard rotational viscometer is probably not ideal because the fluid in the viscometer annular gap between the rotor and the bob may not be totally sheared. The dial readings measured at higher shear rates (preferably above 100 sec^{-1}) may be fit with a non-linear least square regression analysis and extrapolated to a yield point.

The Yield-Power law model combines both the Bingham plastic and Power-law models. It reduces to the Bingham plastic model when flow behavior index, n , is equal to one, and to the Power-law model when yield point, τ_0 , is equal to zero. Viscosity, μ , is a function of shear rate and defined as

$$\mu = \frac{\tau}{\dot{\gamma}} \quad (3.27)$$

By manipulating Eq. 3.24, the non-Newtonian viscosity of the

Yield-Power-law fluids may be expressed as:

$$\mu = \frac{\tau_0}{\dot{\gamma}} + K\dot{\gamma}^{n-1} \quad (3.28)$$

The definition of shear rate (Bird, 1960), $\dot{\gamma}$, in a Cartesian coordinate system is

$$\dot{\gamma} = \left| \sqrt{\left(\frac{\partial v}{\partial x}\right)^2 + \left(\frac{\partial v}{\partial y}\right)^2} \right| \quad (3.29)$$

In bipolar coordinates, with a similar transformation technique (see appendix A), it can be written as:

$$\dot{\gamma} = \left| \frac{\psi}{a} \sqrt{\left(\frac{\partial v}{\partial \epsilon}\right)^2 + \left(\frac{\partial v}{\partial \eta}\right)^2} \right| \quad (3.30)$$

Therefore, the non-Newtonian viscosity in terms of velocity becomes:

$$\mu = \frac{\tau_0}{\left| \frac{\psi}{a} \sqrt{\left(\frac{\partial v}{\partial \epsilon}\right)^2 + \left(\frac{\partial v}{\partial \eta}\right)^2} \right|} + K \left| \frac{\psi}{a} \sqrt{\left(\frac{\partial v}{\partial \epsilon}\right)^2 + \left(\frac{\partial v}{\partial \eta}\right)^2} \right|^{n-1} \quad (3.31)$$

When the above equation is substituted into Eq. 3.22, The governing equation of motion for the Yield-Power law fluids in eccentric annulus is derived. Before solving this cumbersome equation, dimensionless parameters are introduced to simplify

the equation and make the solution more general.

3.5 Dimensional Analysis

Let us introduce two dimensionless groups, namely, dimensionless velocity and dimensionless frictional pressure loss gradient. They are defined as:

$$v_D = \frac{v}{\left(\frac{K}{\rho r_o^n}\right)^{\frac{1}{2-n}}} \quad (3.32)$$

$$f = \left(\frac{\Delta P_f}{\Delta L}\right)_D = \frac{\frac{\Delta P_f}{\Delta L}}{\left(\frac{K^2}{\rho^n r_o^{n+2}}\right)^{\frac{1}{2-n}}} \quad (3.33)$$

The velocity profile of laminar flowing fluids is independent of density. However, a dummy term, ρ , which has units of density is included in dimensionless groups so that dimensionless velocity is not a direct function of $\Delta P_f / \Delta L$. With this set of dimensionless groups, we will be able to evaluate constant flow rate cases. Obviously, the final solution will be independent of the value of ρ .

Substituting the above Eqs. 3.32 and 3.33 into Eq. 3.22 with Eq. 3.31, a dimensionless form of the governing equation of motion is obtained. The intermediate steps of this derivation are provided in Appendix B. After dimensional analysis, the equation of motion becomes

$$\left(\frac{\sinh \varepsilon_0}{\psi}\right)^2 f + \frac{\partial}{\partial \varepsilon} \left(\mu_D \frac{\partial v_D}{\partial \varepsilon} \right) + \frac{\partial}{\partial \eta} \left(\mu_D \frac{\partial v_D}{\partial \eta} \right) = 0 \quad (3.34)$$

and allows for the following dimensionless groups:

$$\mu_D = \left(\frac{\rho^{n-1} r_0^{2n-2}}{K} \right)^{\frac{1}{2-n}} \mu = \frac{\tau_D}{\gamma_D} \sinh \varepsilon_0 + \left(\frac{\gamma_D}{\sinh \varepsilon_0} \right)^{n-1} \quad (3.35)$$

$$\tau_D = \frac{\tau_0}{\left(\frac{K^2}{\rho^n r_0^{2n}} \right)^{\frac{1}{2-n}}} \quad (3.36)$$

$$\gamma_D = \left| \psi \sqrt{\left(\frac{\partial v_D}{\partial \varepsilon} \right)^2 + \left(\frac{\partial v_D}{\partial \eta} \right)^2} \right| \quad (3.37)$$

Now the equation of motion, Eq. 3.34, needs to be solved for dimensionless velocity and viscosity profiles, and this velocity profile can be numerically integrated to obtain a dimensionless flow rate defined as

$$Q_D = \int_0^{2\pi} \int_{\varepsilon_0}^{\varepsilon_1} v_D \left(\frac{\sinh \varepsilon_0}{\psi} \right)^2 \partial \varepsilon \partial \eta \quad (3.38)$$

then

$$Q = r_0^2 \left(\frac{K}{\rho r_0^n} \right)^{\frac{1}{2-n}} Q_D . \quad (3.39)$$

✱

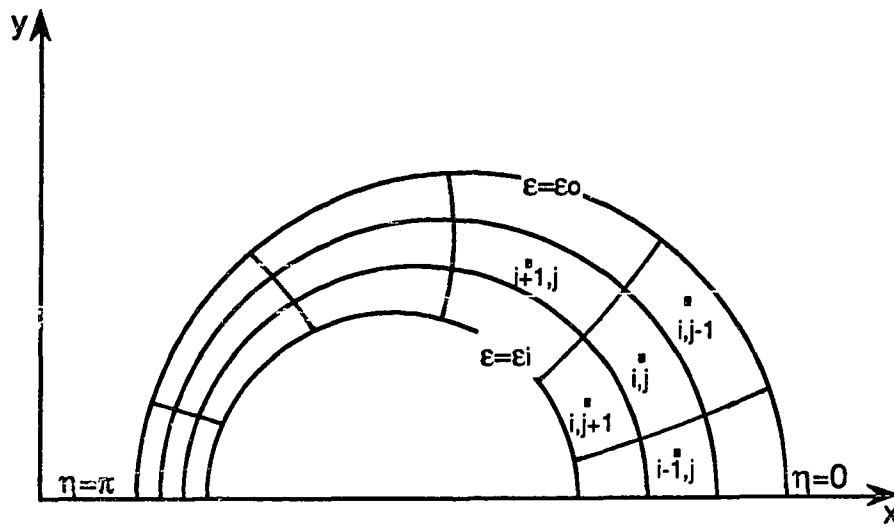
A solution technique to this mathematical model is presented in the next chapter.

CHAPTER IV

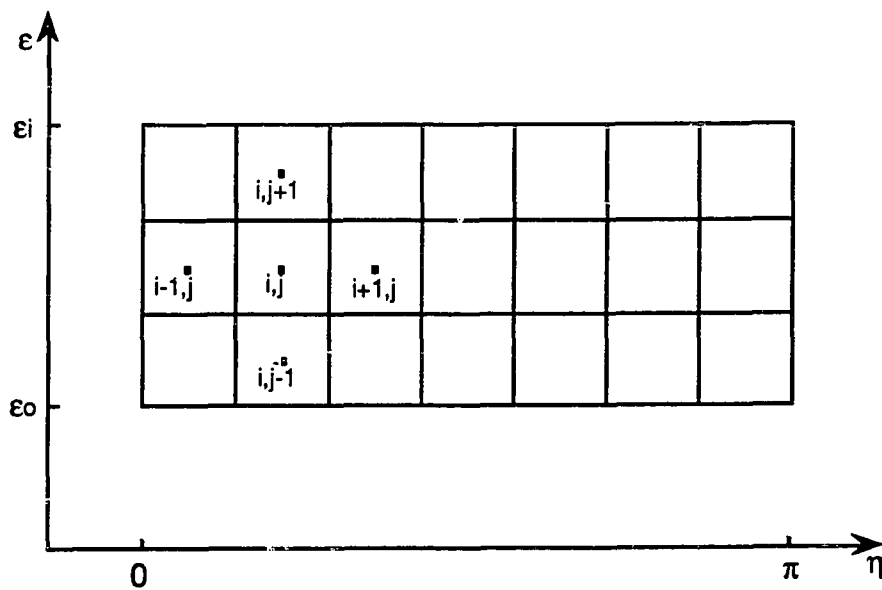
NUMERICAL MODEL

A numerical model based on a finite difference calculation technique will be developed to solve the equation of motion (Eq. 3.34). Many techniques such as the discretization method and the solution of the algebraic equations used in this chapter are given by Patankar (1983).

In an eccentric annulus, the axis that goes through the center points of the inner and outer pipes is the line-of-symmetry which divides the velocity profile into two identical parts. Therefore, we shall solve for the velocity profile only in one half of the eccentric annulus to keep the calculations to a minimum. In order to apply the finite difference technique, the annular region will be subdivided into a grid network. Figure 4.1 shows the grid network in bipolar coordinates and the transformed coordinates. The convenience of this transformation is that the eccentric annular region may be treated as a rectangular region which is much easier to handle with the finite difference methods. Here we will present a numerical solution of the equation of motion so that the distribution of velocity, v_D , can be constructed. The numerical method replaces the continuous information contained in the exact solution of the differential equation with discrete values.



(a)



(b)

Fig. 4.1 Eccentric annulus in: (a) bipolar coordinates
(b) transformed coordinates

4.1 Discretization of the Equation of Motion

A discretization equation, an algebraic relationship relating the values of velocity, will be derived from the differential equation of motion and thus will express the same physical information as the differential equation itself. A discretization method called control-volume formulation will be used such that the resulting discretization will be consistent over a small region surrounding a grid point. Now, let us recall the transformed equation of motion before we start discretization:

$$\left(\frac{\sinh \epsilon_0}{\psi}\right)^2 f + \frac{\partial}{\partial \epsilon} \left(\mu_D \frac{\partial v_D}{\partial \epsilon} \right) + \frac{\partial}{\partial \eta} \left(\mu_D \frac{\partial v_D}{\partial \eta} \right) = 0 \quad (4.1)$$

To derive the discretization equation, the grid-point cluster shown in Fig. 4.2 is used. Attention is focused on the grid-point, P, which has the grid-points N, E, S, and W as its neighbors. The dashed lines show the face of the control-volume. The subscript D (denoting the dimensionless parameters) will be ignored from now on to keep the length of the equation to a minimum. Integration over the control-volume results in:

$$\iint \left(\frac{\sinh \epsilon_0}{\psi}\right)^2 f \, \partial \epsilon \partial \eta + \iint \frac{\partial}{\partial \epsilon} \left(\mu \frac{\partial v}{\partial \epsilon} \right) \partial \epsilon \partial \eta + \iint \frac{\partial}{\partial \eta} \left(\mu \frac{\partial v}{\partial \eta} \right) \partial \epsilon \partial \eta = 0 \quad (4.2)$$

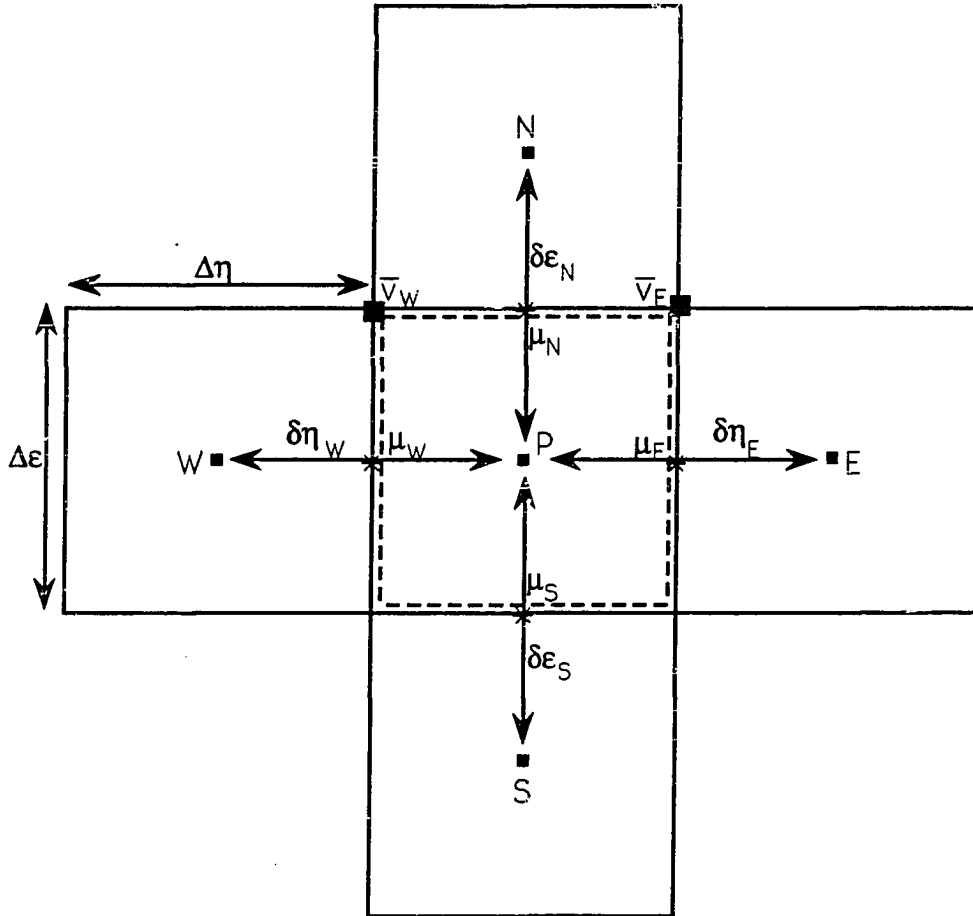


Fig. 4.2 Grid-point cluster

A profile assumption is necessary at this point. The piecewise-linear profile will be used between grid-points. Figure 4.3 shows the piecewise-linear profile of velocity in η -direction. Evaluating the derivatives in Eq. 4.2, using the piecewise-profile, and expanding the equation, we have:

$$\left(\frac{\sinh \epsilon_0}{\psi}\right)^2 f \Delta\epsilon \Delta\eta + \left[\mu_N \left(\frac{V_N - V_P}{\delta\epsilon_N} \right) - \mu_S \left(\frac{V_P - V_S}{\delta\epsilon_S} \right) \right] \Delta\eta + \left[\mu_E \left(\frac{V_E - V_P}{\delta\eta_E} \right) - \mu_W \left(\frac{V_P - V_W}{\delta\eta_W} \right) \right] \Delta\epsilon = 0 \quad (4.3)$$

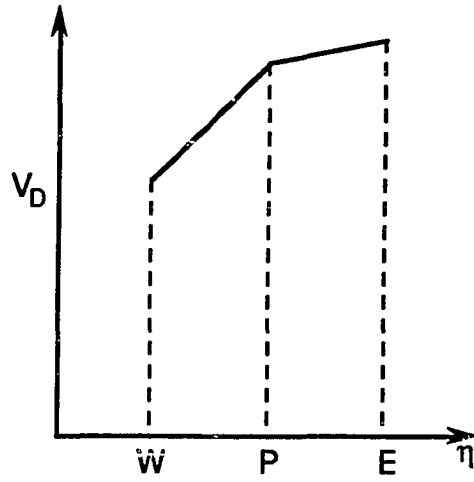


Fig. 4.3 Piecewise-linear profile

It is convenient to cast the discretization equation into the following form:

$$\alpha_P V_P = \alpha_N V_N + \alpha_S V_S + \alpha_E V_E + \alpha_W V_W + \beta \quad (4.4)$$

Further expansion of Eq. 4.3 and grouping of its terms as in Eq. 4.4, defines the discretization equation constants,

$$\alpha_N = \mu_N \frac{\Delta \eta}{\delta \epsilon_N} \quad (4.5)$$

$$\alpha_S = \mu_S \frac{\Delta \eta}{\delta \epsilon_S} \quad (4.6)$$

$$\alpha_E = \mu_E \frac{\Delta \epsilon}{\delta \eta_E} \quad (4.7)$$

$$\alpha_W = \mu_W \frac{\Delta \epsilon}{\delta \eta_W} \quad (4.8)$$

$$\alpha_P = \alpha_N + \alpha_S + \alpha_E + \alpha_W \quad (4.9)$$

$$\beta = \left(\frac{\sinh \epsilon_0}{\psi} \right)^2 f \Delta \epsilon \Delta \eta \quad (4.10)$$

A set of discretization equations for non-Newtonian viscosity terms, μ_N , μ_S , μ_E , and μ_W , also needs to be derived. Note that velocities are calculated at the center of each grid while the viscosities will be computed at the control-volume faces. A similar technique to the above discretization procedure may be used to discretize the viscosity equation derived in Chapter III. The equation of non-Newtonian viscosity at the north face of the control-volume (from Eqs. 3.35 and 3.37) is:

$$\mu_N = \frac{\tau_D}{\gamma_N} \sinh \epsilon_0 + \left(\frac{\gamma_N}{\sinh \epsilon_0} \right)^{n-1} \quad (4.11)$$

$$\text{where } \gamma_N = \left| \psi \sqrt{\left(\frac{\partial v}{\partial \epsilon} \right)^2 + \left(\frac{\partial v}{\partial \eta} \right)^2} \right|$$

Noting the location of μ_N in Fig. 4.2, $\partial v / \partial \epsilon$ and $\partial v / \partial \eta$ need to be discretized. For example, the first derivative of velocity with respect to ϵ for μ_N may simply be discretized as:

$$\frac{\partial v}{\partial \epsilon} = \frac{v_N - v_P}{\delta \epsilon_N} \quad (4.12)$$

In order to do the same for $\partial v / \partial \eta$, the velocities on the upper right and left corners of the P grid are needed.

$$\frac{\partial v}{\partial \eta} = \frac{\bar{v}_W - \bar{v}_E}{\Delta \eta_P} \quad (4.13)$$

\bar{v}_W and \bar{v}_E are calculated by averaging the velocities at the centers of the surrounding grids. Now, if Eqs. 4.12 and 4.13 are combined with 4.11, the viscosity term north of point P is derived.

$$\mu_N = \frac{\tau_D}{\gamma_N} \sinh \epsilon_0 + \left(\frac{\gamma_N}{\sinh \epsilon_0} \right)^{n-1} \quad (4.14)$$

$$\text{where } \gamma_N = \left| \psi \sqrt{\left(\frac{v_N - v_P}{\delta \epsilon_N} \right)^2 + \left(\frac{\bar{v}_W - \bar{v}_E}{\Delta \eta_P} \right)^2} \right|$$

The other viscosity terms may also be discretized in a similar manner.

4.2 The Boundary Conditions

Figure 4.4 shows the complete grid network of the eccentric annular region. The boundaries of the region are the inner pipe (ϵ_i), the outer pipe (ϵ_o), and the line-of-symmetry ($\eta=0$ and π). The

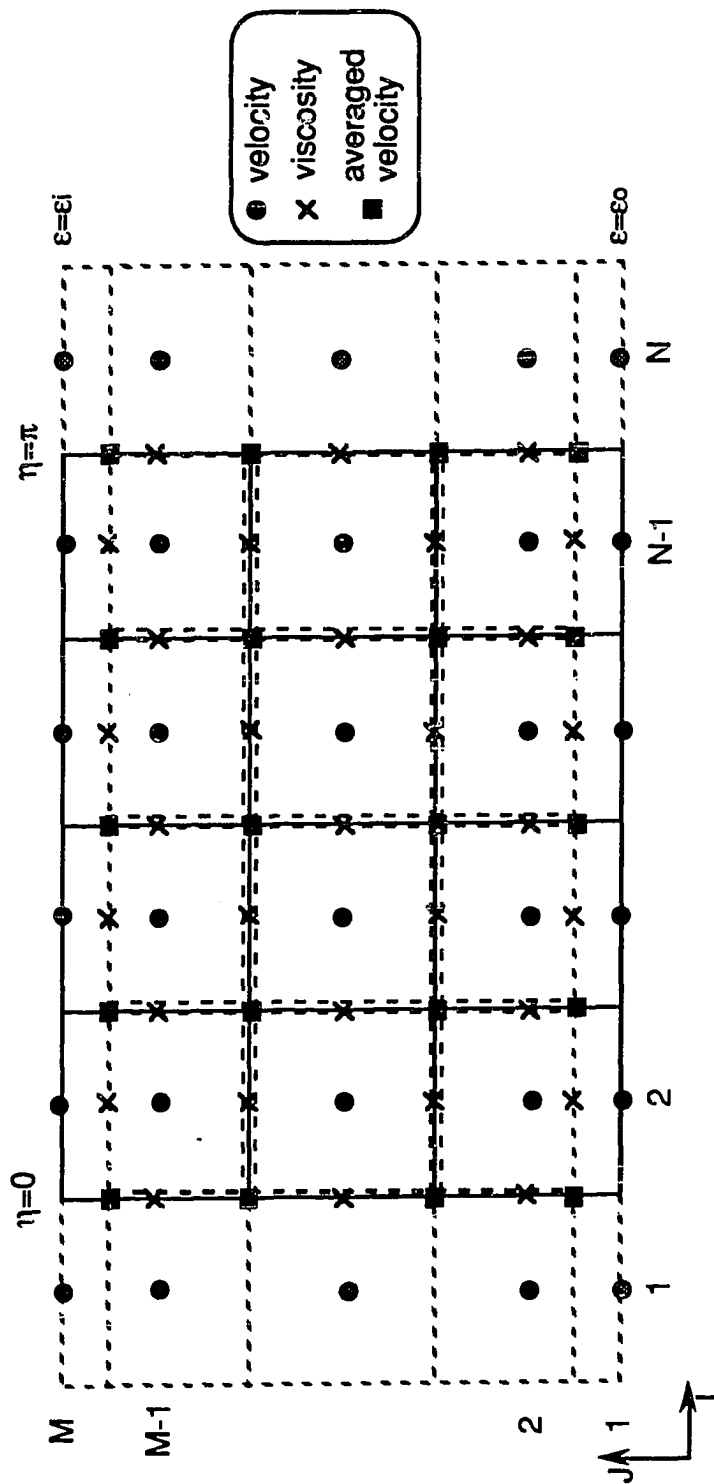


Fig. 4.4 The grid network

boundary conditions, assuming no slip at the pipe walls, are:

$$v = 0 \quad @ \quad \varepsilon = \varepsilon_i \text{ and } \varepsilon_o \quad (4.15)$$

and

$$\frac{\partial v}{\partial \eta} = 0 \quad @ \quad \eta = 0 \text{ and } \pi. \quad (4.16)$$

These boundary conditions are implemented by setting the velocity, v , equal to zero along the rows 1 and M (where $\varepsilon = \varepsilon_o$ and ε_i , respectively) and setting the velocities along the columns 1 and N equal to the velocities along the columns 2 and $N-1$, respectively ($\partial v / \partial \eta = 0$). In Figure 4.4, the dashed lines show the control-volumes. Note that the control-volumes near the pipe walls are smaller; thus, $\delta\varepsilon_N$ s neighboring ε_i and $\delta\varepsilon_S$ s neighboring ε_o will be only half of $\Delta\varepsilon$.

4.3 Solution of the Discretized Equation

To solve for the velocity distribution in the grid network, an iterative method is used. We start from a guessed velocity field and use the discretization equation to obtain an improved field. This procedure is repeated until a solution sufficiently close to the correct solution is reached. However, many techniques may be implemented to solve the algebraic discretization equation, here, the line-by-line method is used. In this method a line (a

row or a column) in the grid network is chosen at a time (Fig. 4.5). Using the latest values of the velocities along the neighboring lines, the velocities along the chosen line are updated. This procedure is used for all the lines (from column 2 to N-1) in the η -direction until the whole grid network is swept. Each sweeping of the grid network is called "one iteration" and yields an improved velocity profile.

For the solution of the velocities along the chosen lines, the Tri-Diagonal-Matrix Algorithm (TDMA) is employed. For convenience in presenting the algorithm, it is necessary to use a somewhat different nomenclature to express the discretization equation (Eq. 4.4). We restructure the Eq. 4.4 in the following form:

$$A_j v_j = B_j v_{j+1} + C_j v_{j-1} + D_j \quad (4.17)$$

for $J = 1, 2, 3, \dots M$. Points 1 and M represent the boundary points on each line. To calculate the velocity, v_j , at any grid along the chosen line, the information from surrounding grids is necessary. v_{j+1} and v_{j-1} are the neighboring grids along the same line. Constants A_j , B_j , and C_j contain information about grids P, N, and S, respectively, while the rest of the information from the neighboring lines and boundaries are collected in D_j . Rearranging the terms of the discretization equation in the form of equation 4.17 defines the constants A_j , B_j , C_j and D_j ,

$$A_j = \alpha_P \quad (4.18)$$

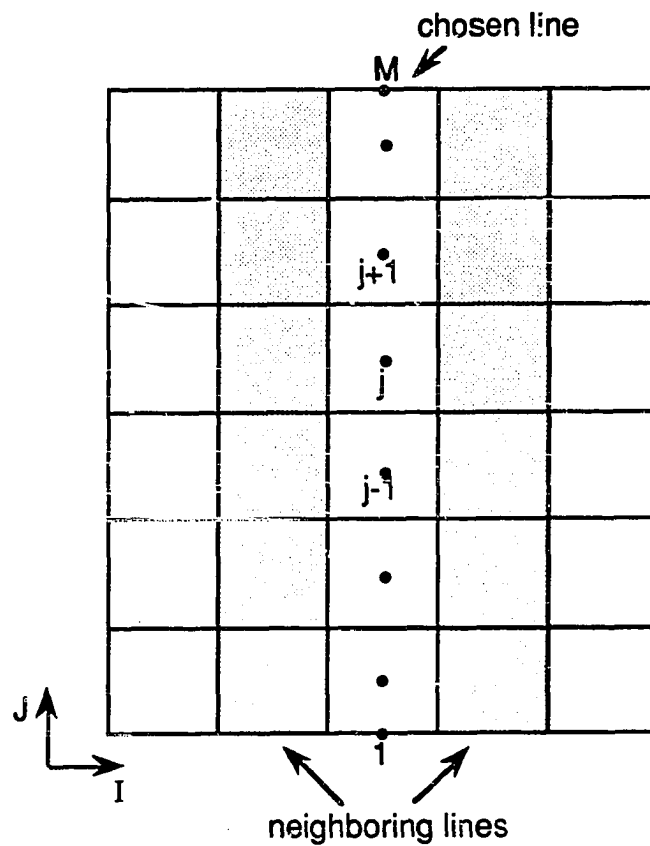


Fig. 4.5 Line-by-line method

$$B_j = \alpha_N \quad (4.19)$$

$$C_j = \alpha_S \quad (4.20)$$

$$D_j = \alpha_W V_W + \alpha_E V_E + \beta \quad (4.21)$$

The velocities at the boundaries of the line are known. Now an expression defining the velocity neighboring the boundary in

terms of the boundary velocity is needed (e.g. writing an expression for v_{M-1} in terms of known v_M). Therefore, we seek a relation

$$v_j = P_j v_{j+1} + Q_j \quad (4.22)$$

This can also be written as:

$$v_{j-1} = P_{j-1} v_j + Q_{j-1} \quad (4.23)$$

Substituting Eq. 4.23 into Eq. 4.17, we get:

$$A_j v_j = B_j v_{j+1} + C_j (P_{j-1} v_j + Q_{j-1}) + D_j \quad (4.24)$$

The above equation can be rearranged to appear like Eq. 4.22, to define the coefficients P_j and Q_j ,

$$P_j = \frac{B_j}{A_j - C_j P_{j-1}} \quad (4.25)$$

$$Q_j = \frac{D_j + C_j Q_{j-1}}{A_j - C_j P_{j-1}} \quad (4.26)$$

These are recurrence relations because they give P_j and Q_j in terms of P_{j-1} and Q_{j-1} . In TDMA, all coefficient P 's and Q 's are calculated using the recurrence relations starting from the one end of the line. Once the other end of the line is reached, the

"back-substitution" process can be started to calculate the velocities (Eq. 4.22) along the line using the previously computed P's and Q's.

In summary, the procedure for calculating the velocity distribution is as follows:

1. Use Eq. 3.20 and 3.21 to calculate ϵ_i and ϵ_o
2. Determine $\Delta\epsilon$ and $\Delta\eta$ based on the size of the grid network
3. Set coefficients P and Q to zero at the boundaries ($\epsilon=\epsilon_i$ and ϵ_o)
4. Guess a velocity field
5. Calculate a viscosity field (Eq. 4.14 and so on) based on the latest velocity field
6. Compute coefficients A_j , B_j , C_j and D_j using Eqs. 4.18-4.21
7. Use recurrence equations 4.25 and 4.26 to compute coefficients P and Q from $J=2$ to $M-1$ for each column
8. Calculate a new velocity field employing Eq. 4.22 from $J=M-1$ to 2 (back substitution)
9. Check for convergence comparing old and new velocity fields
10. Repeat from step 5 until the velocity field converges.

CHAPTER V

RESULTS

A computer program in Fortran IV has been written to implement the numerical solution presented in chapter IV. A listing of the computer program can be found in appendix C. Each run of this program takes anywhere from a few CPU sec. to over 10 CPU min. on a time sharing option of an IBM 3090 depending on the viscous properties of the fluid and the size of the grid network. Trial runs have shown that a grid network of 30x20 is a practical minimum for fairly accurate results. As the grid network is made finer, the flow rates predicted at a given frictional pressure loss will increase, approaching exact solution. However, beyond a 40x40 grid network, increases in flow rate are negligibly small. Heavily non-Newtonian fluids, especially those with high yield points, tend to take more computer time to achieve convergence. Before getting into further detail, the model predictions are verified at this point.

5.1 Model Verification

The calculated flow rate vs frictional pressure loss in concentric annulus are compared with existing analytical solutions of Newtonian flow (Lamb, 1932) and non-Newtonian flow, Power law and Bingham plastic (Fredrickson, 1958), and the

results are in good agreement (within 0.5%). This simply shows that the basic structure of the numerical model is working properly.

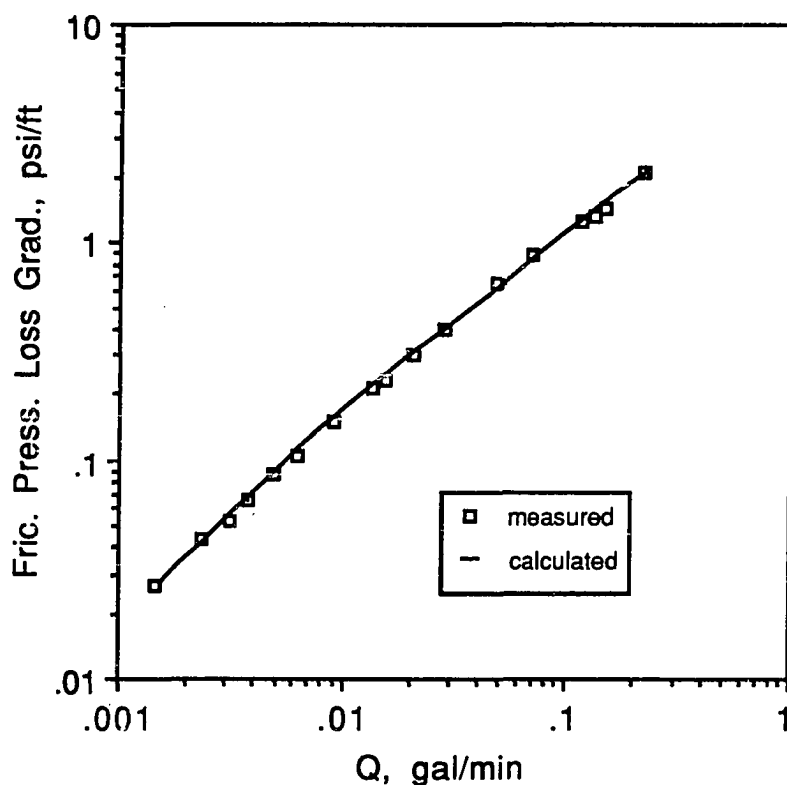


Fig. 5.1 Model verification with CMC solution

Also, the experimental data published by Mitsuishi and Aoyagi (1973) are used to verify the model predictions in eccentric annuli. Using a small scale experimental set-up, these authors

measured the frictional pressure losses of CMC, HEC, and MC solutions. The rheological behavior of these fluids is a best fit by the Sutterby model which is similar to the Yield-Power law model in the sense that it also models shear thinning behavior; however, the Sutterby model differs at very low shear rates where it approaches a constant limiting viscosity, μ_0 .

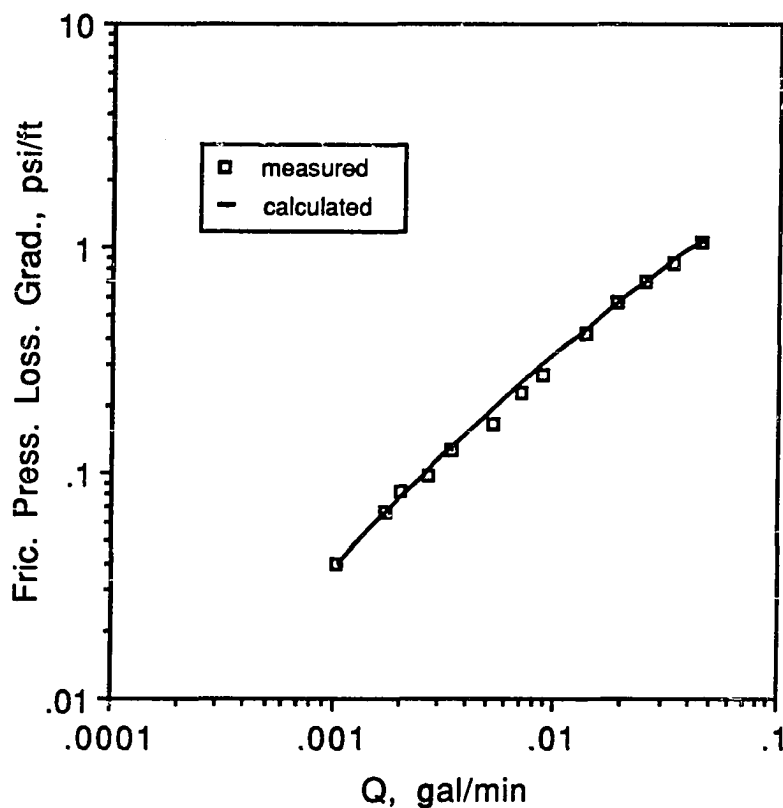


Fig. 5.2 Model verification with HEC solution

Here, the equivalent Yield-Power law model parameters are

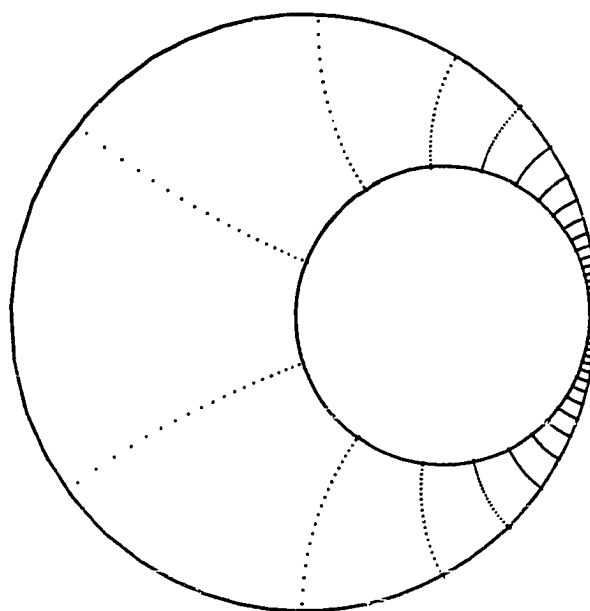
determined for two of these fluids with a limiting viscosity restriction (Table 5.1), and the computer model predictions of frictional pressure losses agree well with the experimental data (Figs. 5.1 and 5.2).

Table 5.1 Fluid properties and geometry of eccentric annuli

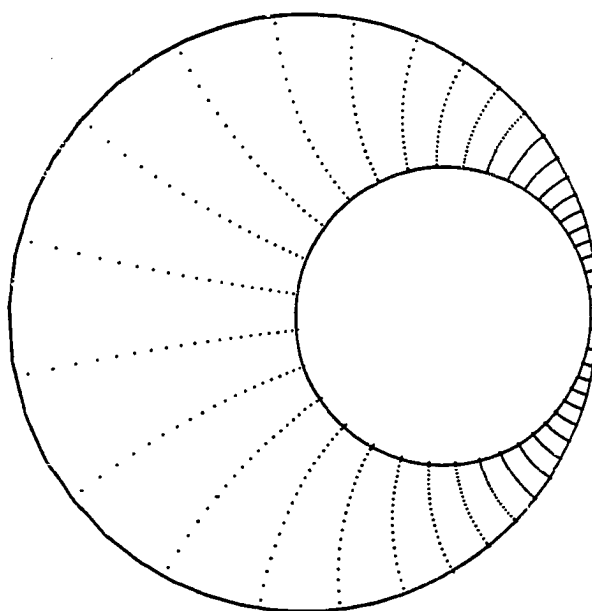
Fluid type	n (d'less)	K (eq. cp)	τ_o (lb/100ft ²)	μ_o (cp)	d_o (in.)	d_i (in.)	e (d'less)
3.92 wt% HEC	0.80	1613	0	1210	0.73	0.46	0.43
3.44 wt% CMC	0.91	4832	14.1	7150	0.60	0.20	0.65

5.2 Velocity Profiles

Previous numerical studies (Redberger, 1962; Guckes, 1975) using bipolar coordinates have divided the eccentric annulus into uniformly distributed grids (constant length grids) in ϵ and η directions. In this study, it is realized that at high eccentricities, a uniformly distributed grid network in bipolar coordinates yields an unrealistic distribution of grid points in physical coordinates. Figure 5.3a shows how grid points are concentrated in the narrow part of the annulus. Since there are very few rows of grids located in the wide part of the annulus,



(a)



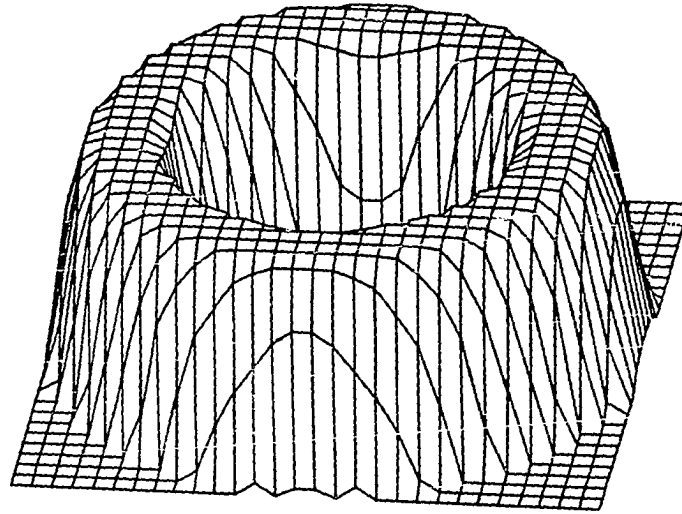
(b)

Fig. 5.3 Distribution of grid points in bipolar coordinates:
(a) uniform, (b) non-uniform

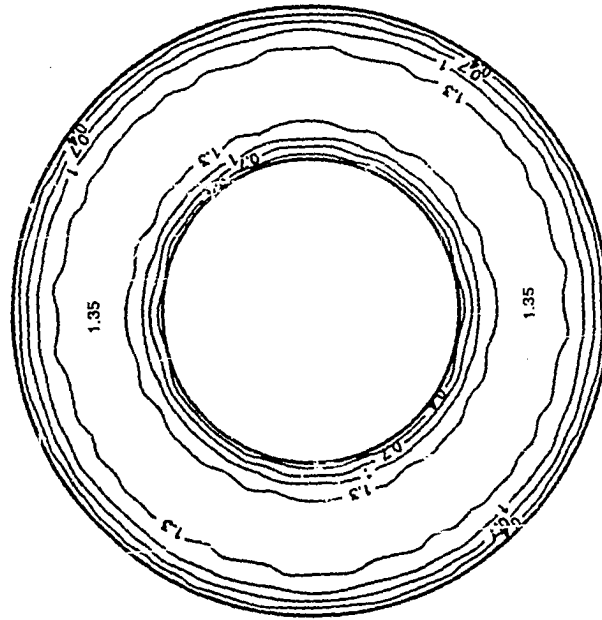
where most of the flow takes place, the point velocity calculations become unstable and consequently inaccurate. To remedy this problem, a non-uniform grid point distribution in η -direction in bipolar coordinates is introduced in this study such that a more realistic distribution of grid points in physical coordinates is obtained (Fig. 5.3b). The algorithm developed (included in appendix C) allows for a uniform distribution of grid points in a concentric annulus but an exponential distribution in a fully eccentric annulus.

Let us now investigate the flow of a Yield-Power law fluid with a flow behavior index, n , of 0.7 and a consistency index, K , of 250 eq. cp and a yield point, τ_o , of 5 lb/100 ft². For a flow rate of 200 gal/min, pipe diameters of 10 and 5 in., the velocity profile of the above fluid in a concentric annulus is shown in Fig. 5.4. Velocity contours are perfectly circular (contour lines in the figures representing fluid flow are not smooth because plots are generated by computer software after smooth data points in bipolar coordinates are extrapolated to a superimposed Cartesian grid network) around the pipes. The velocity of the fluid changes from zero near the walls to a maximum of 1.35 ft/s. This velocity profile is commonly represented by the average velocity which, in this case, is

$$v_{avg} = \frac{Q}{2.448 (d_o^2 - d_i^2)} = \frac{200}{2.448 (10^2 - 5^2)} = 1.09 \text{ ft/s} \quad (5.1)$$

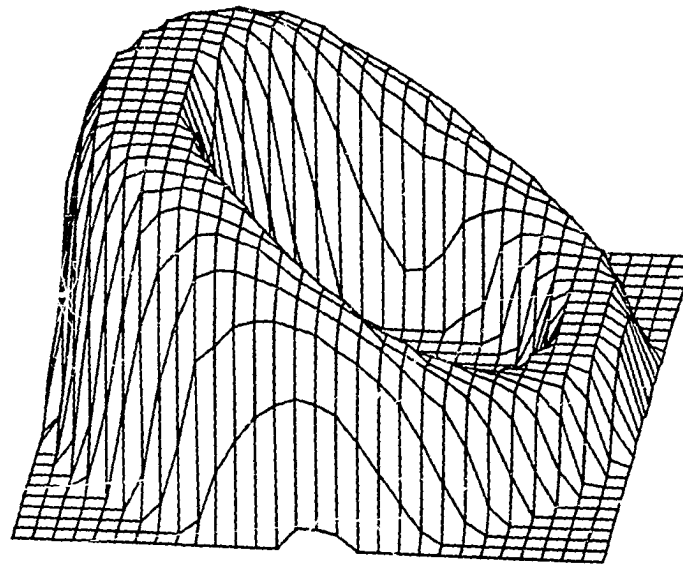


(a)

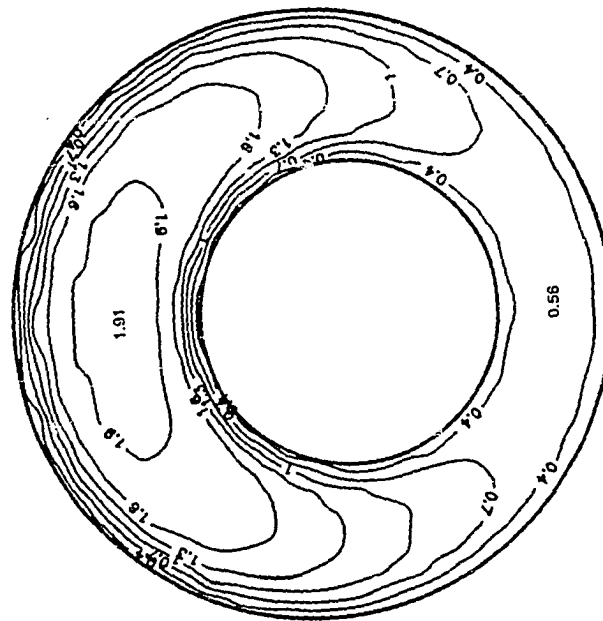


(b)

Fig. 5.4 The Yield-Power law fluid in concentric annulus, $e=0$:
 (a) 3-D velocity profile, (b) 2-D velocity profile



(a)



(b)

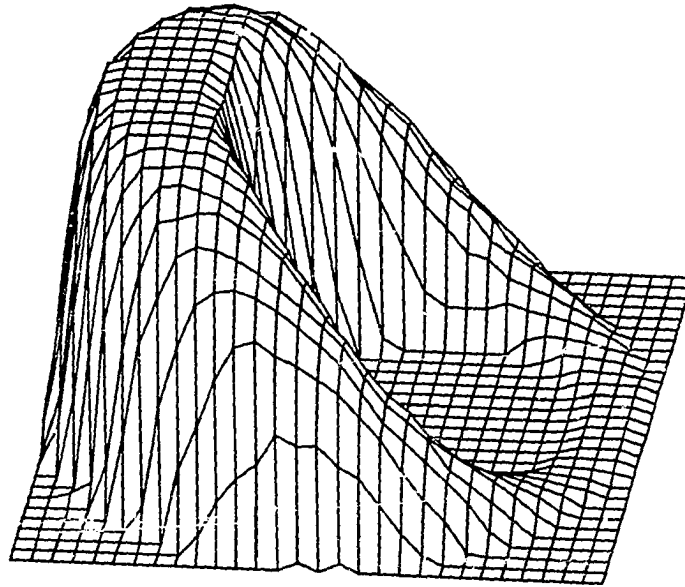
Fig. 5.5 The Yield-Power law fluid in eccentric annulus, $e=0.25$:
 (a) 3-D velocity profile, (b) 2-D velocity profile

The single value representation (average velocity) of this rather simple velocity profile is probably justified. However, as soon as the annulus becomes slightly eccentric, the velocity profile changes considerably (Fig. 5.5). The velocity in the narrowing part of the annulus is reduced because the resistance to flow is increased as the gap between two pipes decreases. Meanwhile, the fluid is rushing into the widening part of the annulus and already traveling at a maximum velocity of 1.91 ft/s while the maximum velocity in the narrow part of the annulus is down to 0.56 ft/s. As eccentricity increases (Figs. 5.6 and 5.7), the flow pattern in Fig. 5.5 is more emphasized so that there is a high velocity plug (flat velocity profile) in the wide part of the annulus while a no flow (stagnant) region is created in the narrow part.

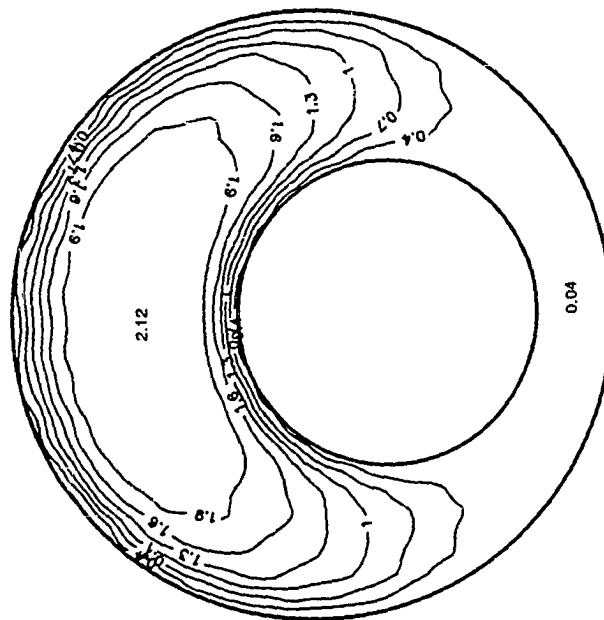
An accurate prediction of the velocity profile is needed for a successful design of mud displacement in cementing operations and cuttings transport in directional drilling. In both cases, the velocity of the fluids in the narrow part of the annulus is an important design criterion. The velocity profile is also needed to correctly predict the travel time of a kick from the bottom of the hole to the surface.

5.3 Viscosity Profiles

An important property of non-Newtonian fluids is that viscosity is a function of shear rate. Then, the existence of a velocity profile implies that there is also a shear rate profile

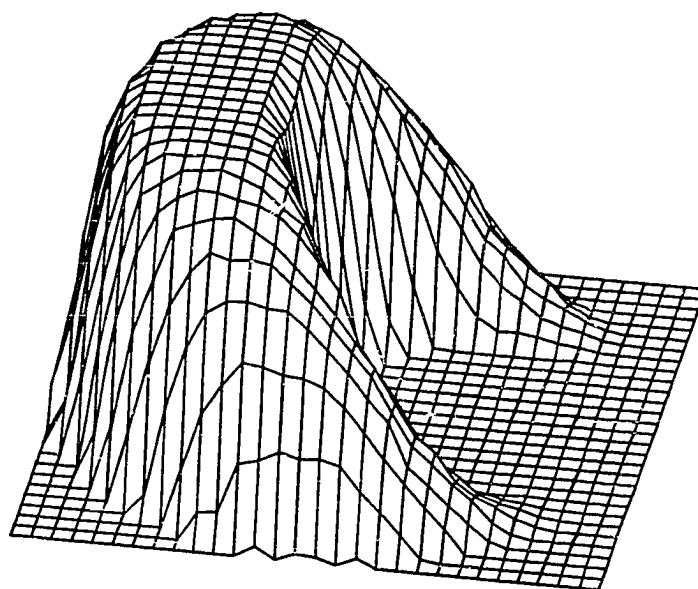


(a)

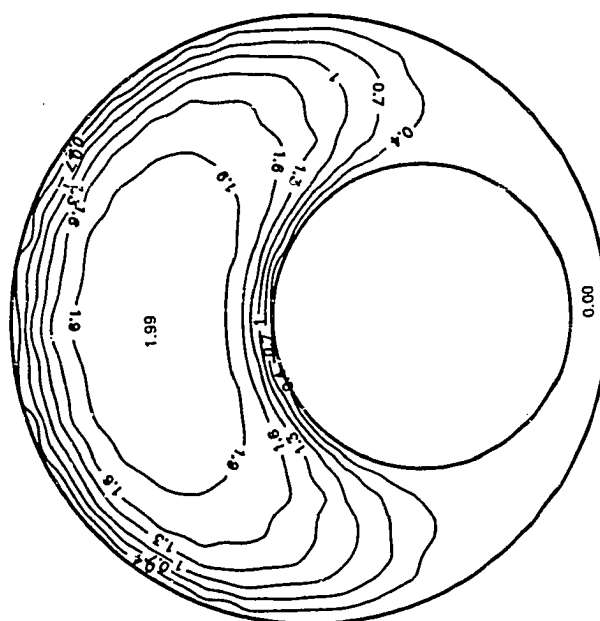


(b)

Fig. 5.6 The Yield-Power law fluid in eccentric annulus, $e=0.5$:
 (a) 3-D velocity profile, (b) 2-D velocity profile



(a)



(b)

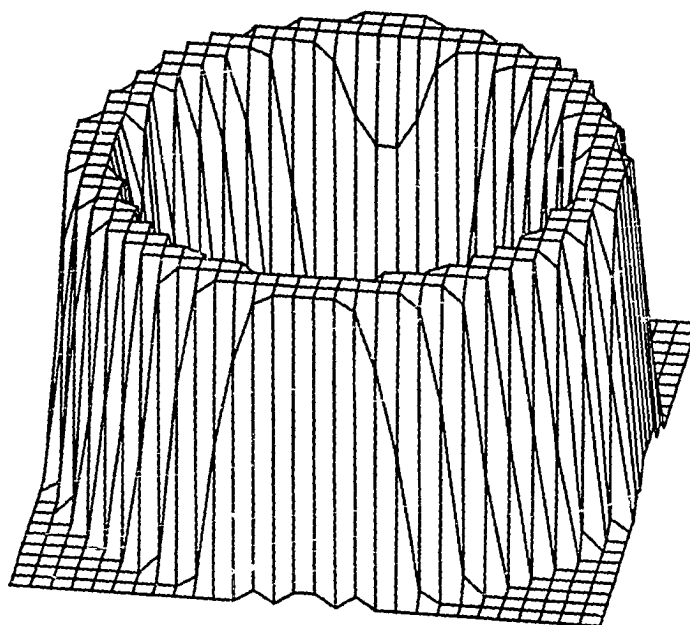
Fig. 5.7 The Yield-Power law fluid in eccentric annulus, $e=0.75$:
 (a) 3-D velocity profile, (b) 2-D velocity profile

and, consequently, a viscosity profile. The local value of viscosity is significant to the drilling engineer in drilled cuttings transport phenomenon. An important parameter is the slip velocity of the cuttings which is directly proportional to the viscosity of the fluid. In the case of non-Newtonian fluids, the variation in viscosity behavior in the annular flow region should be taken into account such that accurate cutting slip behavior can be predicted and the entire phenomenon be better understood. However, just like single value representation of velocity profile, the viscosity profile of non-Newtonian fluids are also represented by a single value term called apparent viscosity (sometimes also called effective viscosity). The apparent viscosity equations for Power law and Bingham plastic fluids, respectively, in a concentric annulus are

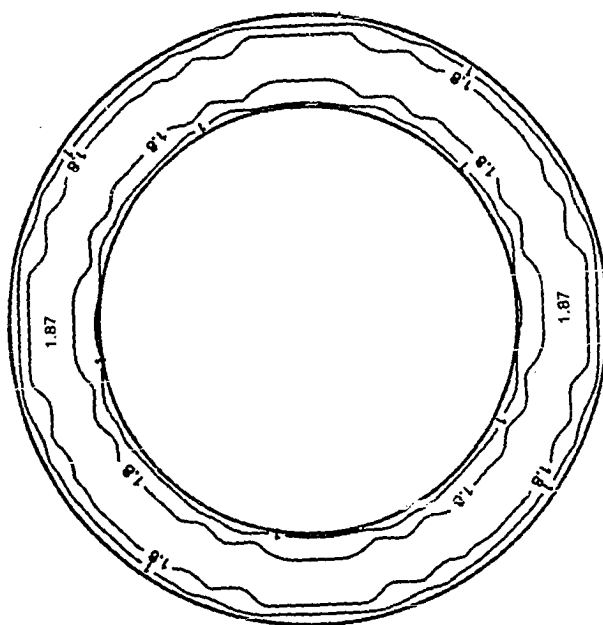
$$\mu_a = \frac{K (d_o - d_i)^{1-n}}{144 v_{avg}^{1-n}} \left(\frac{2 + \frac{1}{n}}{0.0208} \right)^n \quad (5.2)$$

$$\mu_a = \mu_p + \frac{5 \tau_o (d_o - d_i)}{v_{avg}} \quad (5.3)$$

Assume a Bingham Plastic fluid ($n=1$) with a plastic viscosity of 25 cp and a yield point of 10 lb/100 ft². For a flow rate of 200 gal/min in a concentric annulus of pipe diameters of 10 and 7 in., respectively, the velocity profiles of this fluid are similar to the previous case already discussed (Figs. 5.8 and 5.9). Since the annular gap is smaller in this case the effect of eccentricity is



(a)



(b)

Fig. 5.8 The Bingham plastic fluid in concentric annulus, $e=0$:
 (a) 3-D velocity profile, (b) 2-D velocity profile

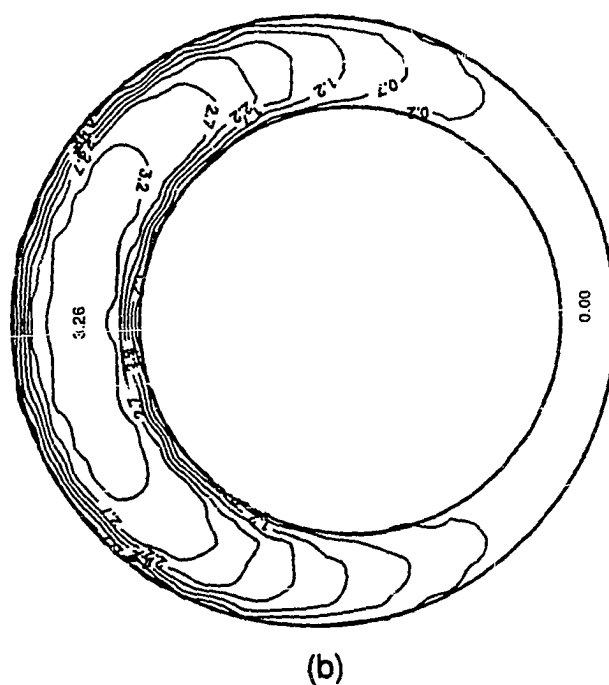
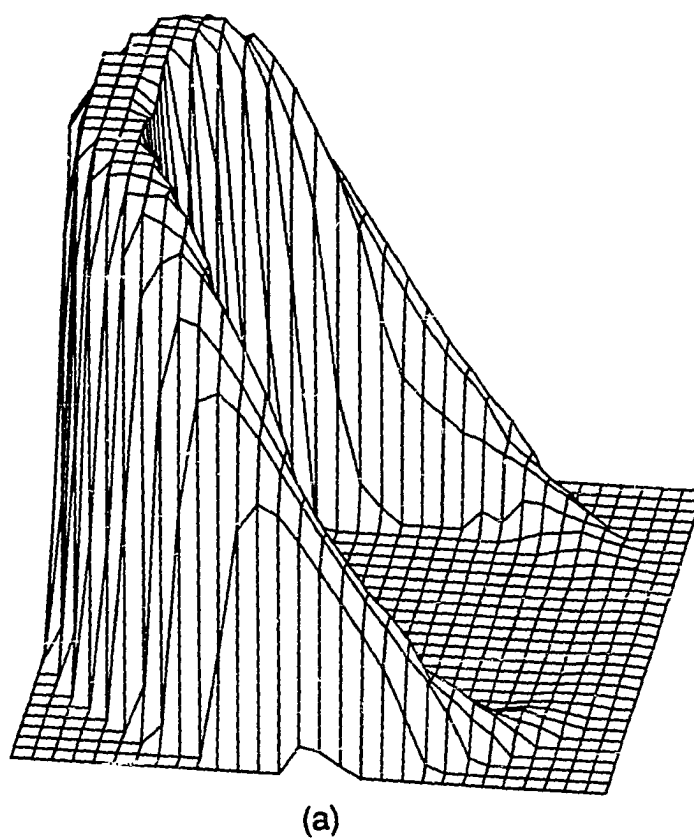


Fig. 5.9 The Bingham plastic fluid in eccentric annulus, $e=0.4$:
 (a) 3-D velocity profile, (b) 2-D velocity profile

more pronounced on the velocity profiles. Of more interest is the viscosity profile (Fig. 5.10) which looks similar to the velocity profile. The viscosity is lower near the pipes and higher in mid annulus. This is expected behavior of shear thinning fluids. A steep velocity profile near the walls (Fig. 5.8) is an indication of high shearing (lower viscosity) while a near flat velocity profile in mid annulus means low shearing (higher viscosity). The apparent viscosity calculated by Eq. 5.3 for this fluid is

$$\mu_a = 25 + \frac{5(10)(10-7)}{1.6} = 119 \text{ cp} \quad (5.4)$$

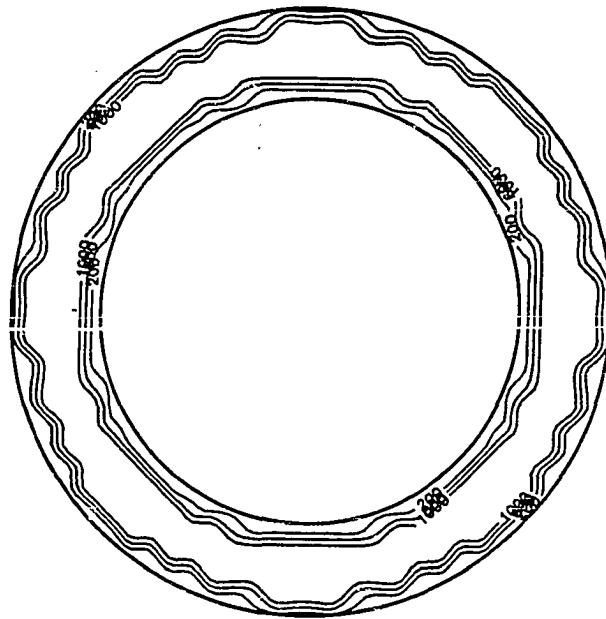


Fig. 5.10 Viscosity profile of the Bingham plastic fluid in concentric annulus

It is important, however, to note that the viscosity profile in most of the annulus is greater than 200 cp. Since most of the flow is in mid annulus (high velocity region), a large percentage of fluid is moving at a viscosity of 1000 cp or more. This is much higher than predicted by Eq. 5.4. This discrepancy between the actual viscosity profile and the apparent viscosities calculated

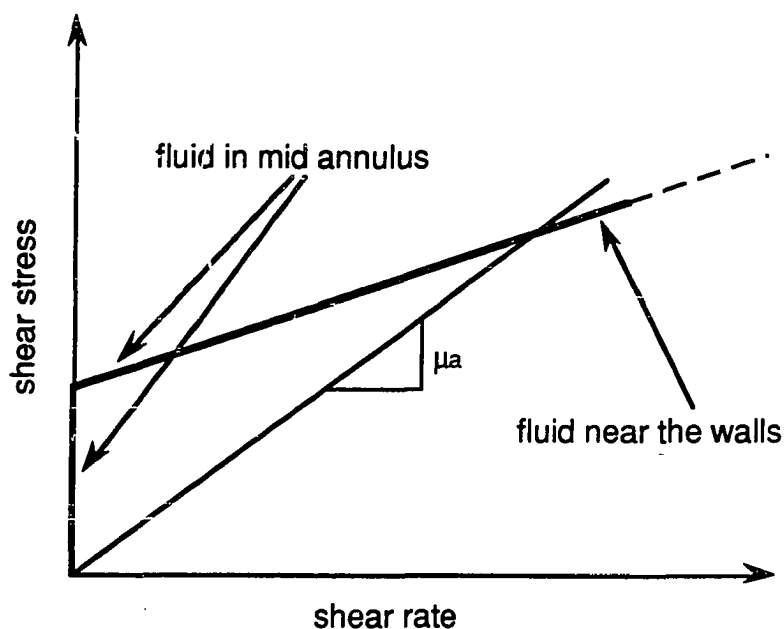


Fig. 5.11 A schematic of where fluids flows on shear curve

by Eqs. 5.2 and 5.3 consistently exist. The reason for it is that the apparent viscosity term is derived by simply equating frictional pressure loss equations of Newtonian and non-Newtonian fluids and solving for Newtonian viscosity. In other words, the apparent viscosity is actually the viscosity of an equivalent Newtonian

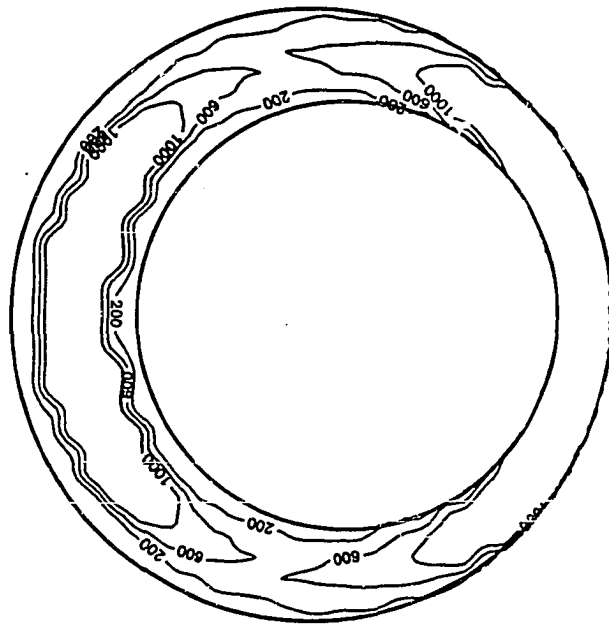


Fig. 5.12 Viscosity profile of the Bingham plastic fluid in eccentric annulus, $e=0.4$

fluid that would exhibit the same frictional pressure loss gradient as the non-Newtonian fluid. Thus, the apparent viscosity has little to do with the actual viscosity behavior of the non-Newtonian fluids. The apparent viscosity concept may mislead the engineer to conclude that the fluid is flowing at a single point on a shear stress vs shear rate curve for a given flow rate. In fact, the elements of fluid experience a continuum of shear rates, dependent on its coordinates in the pipe. The viscosity profile in Fig. 5.10 shows that the fluid is flowing over a wide range of the shear curve (Fig. 5.11). Because the apparent

viscosity is based on the frictional pressure loss gradient, it is always somewhere about the actual viscosities revealed near the pipe walls; therefore, underestimating overall viscosity behavior since most of the fluid travels in the mid annulus region.

When the velocity profile changes with eccentricity (Fig. 5.9), the viscosity profile changes also (Fig. 5.12). Now, there are two high viscosity regions corresponding to two flat velocity profile regions: the first one being the high velocity region and the second the no flow region. It is interesting to note that at 200 gal/min in a narrow annulus, much of the fluid is moving at high viscosity without being sheared.

Table 5.2 Frictional pressure loss gradient data

e (d'less)	$\Delta P_f / \Delta L$ (psi/ft)	R (d'less)
0.00	0.00870	1.00
0.25	0.00820	0.94
0.50	0.00708	0.81
0.75	0.00598	0.69
0.95	0.00528	0.61

5.4 Frictional Pressure Losses

At a constant flow rate, the frictional pressure losses in an annulus decrease with increasing eccentricity. The decrease in

frictional pressure loss in the example case of the Yield–Power law fluid is presented in Table 5.2. R is the ratio of frictional pressure losses in eccentric annulus to concentric annulus. At an eccentricity of 0.95, frictional pressure loss is about 61% of what it was in concentric annular flow.

5.4.1 A Correlation of Frictional Pressure Loss

For *Power-law* fluids, using Eqs. 3.33 and 3.39, it can be shown that:

$$Q = \left(\frac{\Delta P_f}{\Delta L} \frac{r_o^{3n+1}}{K} \right)^{\frac{1}{n}} Q_D \quad (5.5)$$

For a given value of d_i/d_o , n , e , the model calculates a dimensionless flow rate, Q_D . Q_{Dc} and Q_{De} are the dimensionless flow rates for a concentric and an eccentric annulus, respectively. Evaluating a constant flow rate case, Eq. 5.5 can be written as

$$Q = \left[\left(\frac{\Delta P_f}{\Delta L} \right)_c \frac{r_o^{3n+1}}{K} \right]^{\frac{1}{n}} Q_{Dc} \quad (5.6a)$$

and

$$Q = \left[\left(\frac{\Delta P_f}{\Delta L} \right)_e \frac{r_o^{3n+1}}{K} \right]^{\frac{1}{n}} Q_{De} \quad (5.6b)$$

Simultaneous solution of Eqs. 5.6a and 5.6b yields:

$$R = \frac{\left(\frac{\Delta P_f}{\Delta L}\right)_e}{\left(\frac{\Delta P_f}{\Delta L}\right)_c} = \left(\frac{Q_{dc}}{Q_{de}}\right)^n \quad (5.7)$$

Now, R can be expressed in terms of the dimensionless flow rate calculated by the computer model. For Power law fluids, R is a function of pipe diameter ratio, flow index behavior and eccentricity (Figs. 5.13-5.16).

These figures show that at a constant flow rate the frictional pressure losses decrease as eccentricity increases. As fluids are more shear thinning (decreasing n), their velocity profiles in the wide and narrow parts of the annulus become flatter; thus, increasing their overall viscosity. Consequently, these fluids are subject to less reduction in frictional pressure losses in eccentric annulus. It can also be seen in Figs. 5.13-5.16 that reduction in frictional pressure loss is more substantial in narrower annulus (d_i/d_o approaching 1). When d_i/d_o approaches zero (pipe flow), the effect of eccentricity on R diminishes as expected.

The data used to generate these figures are fitted with a simple equation using non-linear regression analysis. The equation is valid for eccentricities from 0 to 0.95 and pipe diameter ratios of 0.3 to 0.9 and flow behavior index of 0.4 to 1.0;

$$R = 1 - 0.072 \frac{e}{n} \left(\frac{d_i}{d_o}\right)^{0.8454} - 1.5 e^2 \sqrt{n} \left(\frac{d_i}{d_o}\right)^{0.1852} + 0.96 e^3 \sqrt{n} \left(\frac{d_i}{d_o}\right)^{0.2527} \quad (5.8)$$

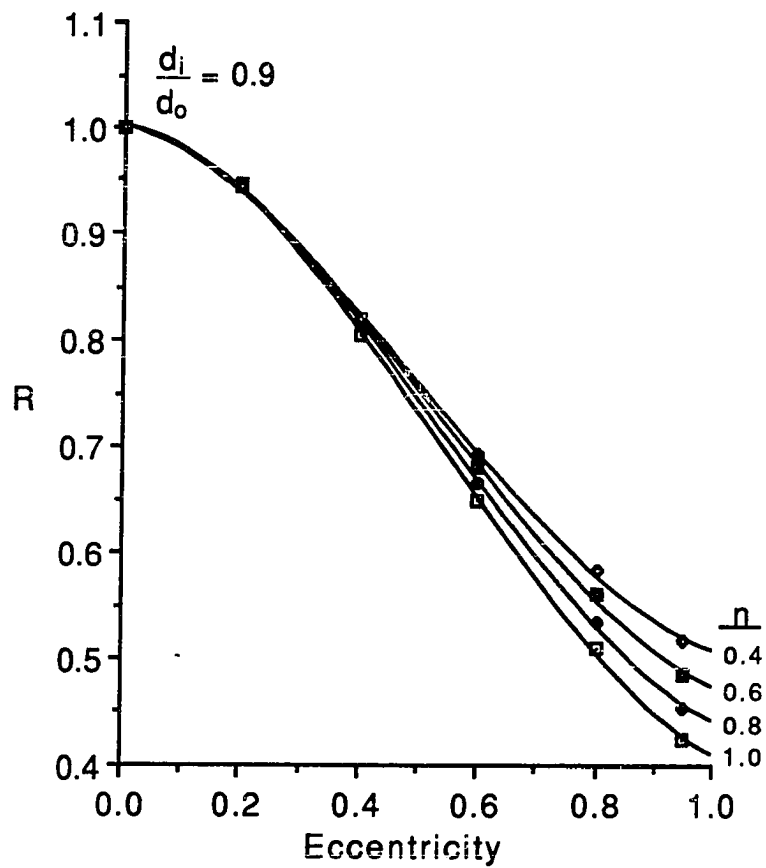


Fig. 5.13 Reduction in frictional pressure loss gradient in an annulus of pipe ratio of 0.9

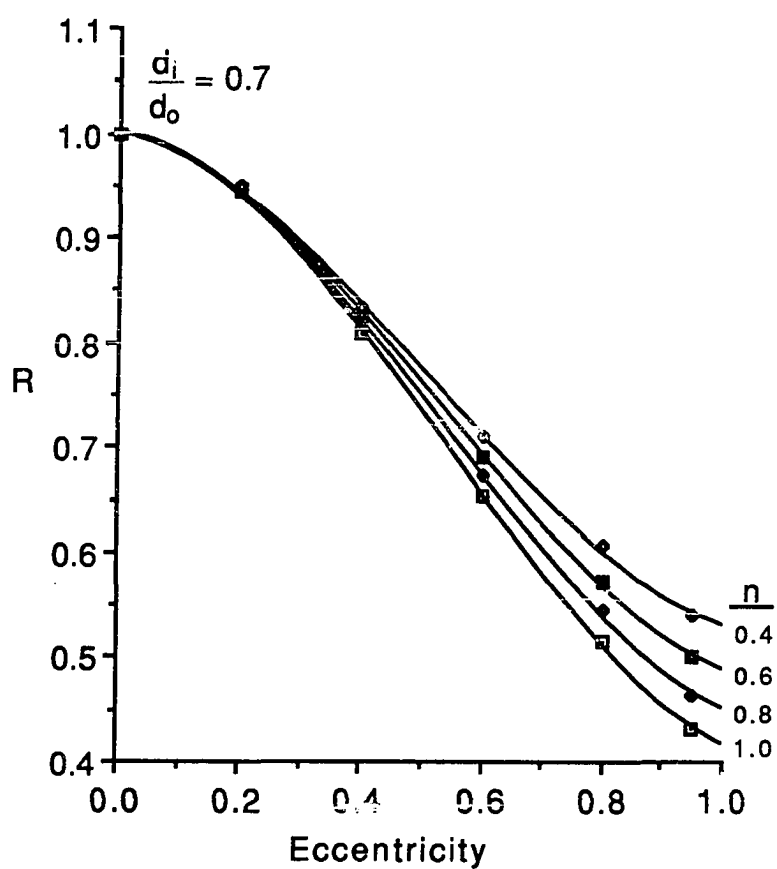


Fig. 5.14 Reduction in frictional pressure loss gradient in an annulus of pipe ratio of 0.7

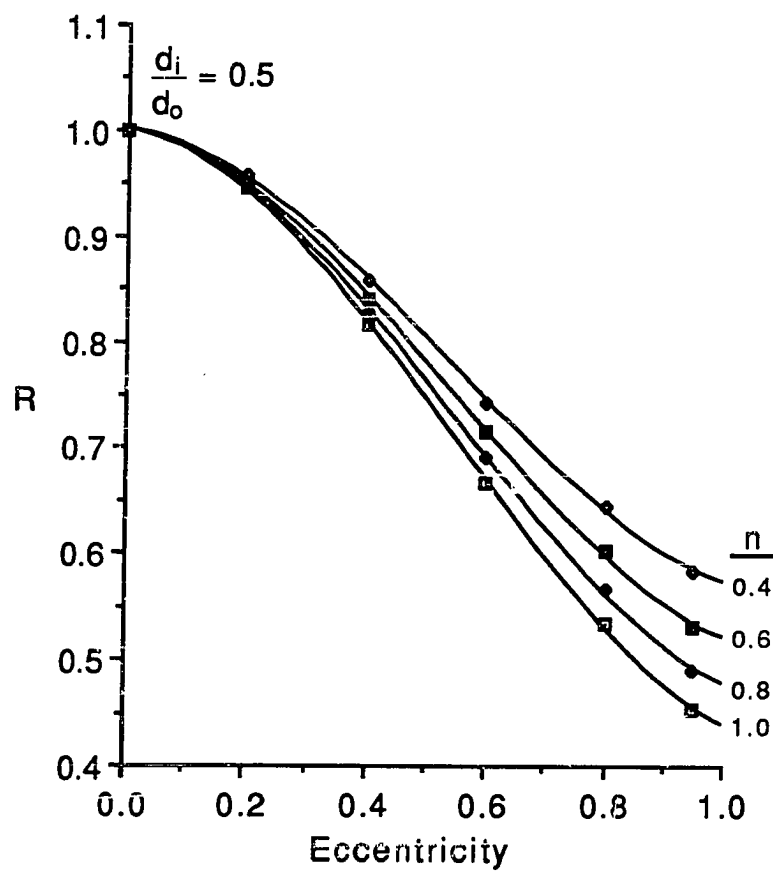


Fig. 5.15 Reduction in frictional pressure loss gradient in an annulus of pipe ratio of 0.5

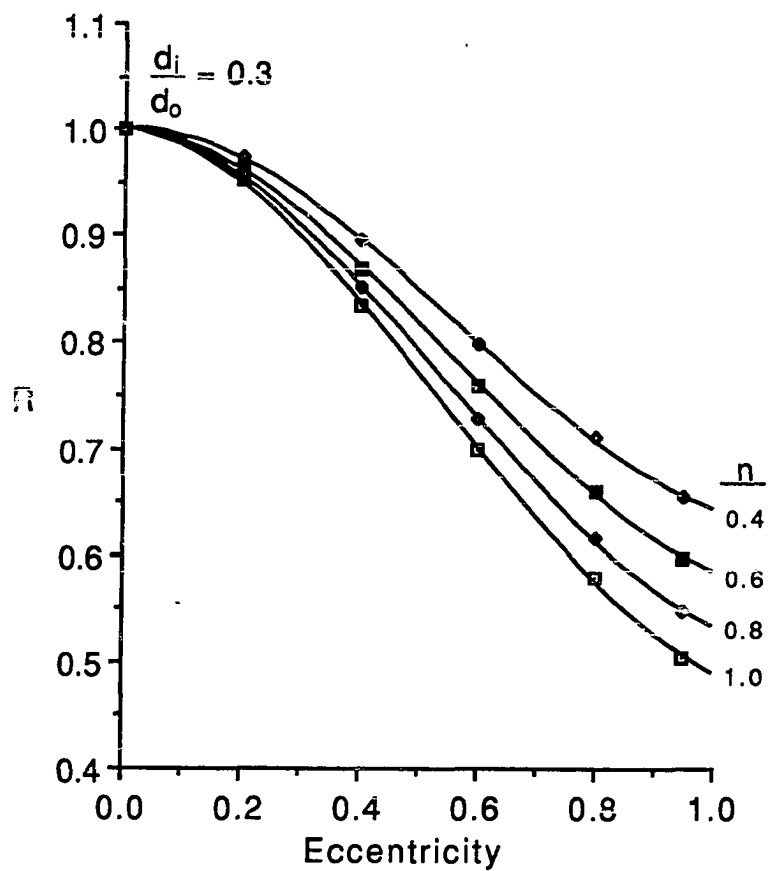


Fig. 5.16 Reduction in frictional pressure loss gradient in an annulus of pipe ratio of 0.3

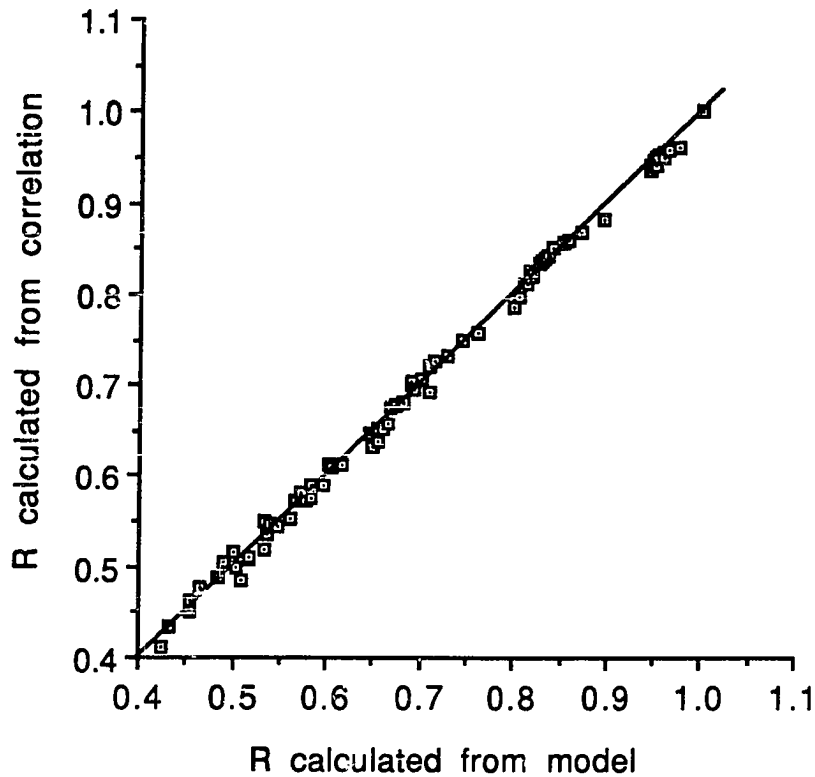


Fig. 5.17 Correlation accuracy

This correlation is accurate within $\pm 5\%$ (Fig. 5.17). To predict frictional pressure loss gradient in an eccentric annulus, calculate the frictional pressure loss gradient in concentric annulus and R using Eq. 5.8, then:

$$\left(\frac{\Delta P_f}{\Delta L}\right)_e = \left(\frac{\Delta P_f}{\Delta L}\right)_c R \quad (5.9)$$

Similar correlations for Bingham plastic and Yield-Power law fluids may also be constructed from the results of the model. However, the computing time will be considerably longer for such fluids.

CHAPTER VI

APPLICATIONS

In Chapter V, the eccentric annular model developed in previous chapters was shown to predict velocity profiles, viscosity profiles, and frictional pressure losses of non-Newtonian fluids. This model can also be used as a base in simulating selected annular flow related drilling engineering problems, such as cuttings transport, kick displacement, surge pressure calculations, and simulation of casing reciprocation.

In this chapter two relatively simpler problems, the surge pressure calculation case and kick displacement case are investigated. The intention is to show how to apply the model and to introduce generally neglected eccentricity to the two problems. The first problem to be addressed is the surge pressure calculations caused by a closed-end pipe such as a casing string in a well. The second is the displacement of a gas kick in solution in an oil-base mud.

6.1 Surge Pressure Calculations

Pulling or running a pipe string causes changes in the pressure exerted by the mud column on the open hole formations. Positive pressure surges created by running a casing string into the hole can fracture weak formations and cause lost circulation

while negative pressure surges created by pulling a casing string can reduce bottom hole pressure such that fluid bearing formations can flow into the wellbore and cause well control problems. The need for calculating surge pressures has long been recognized in the industry and several steady-state (Burkhardt, 1961; Shuch, 1964; Fontenot, 1974) and unsteady-state (Lubinski, 1977; Lal, 1983; Mitchell, 1988a) models of this phenomenon exist in the literature.

In a comparative study of the steady-state and the unsteady-state models of surge pressure calculations, Mitchell (1988b) points out that the steady-state models are conservative in their prediction of surge pressure calculations because, unlike the unsteady-state models (also called dynamic models), several factors are not considered, such as fluid compressibility, fluid inertia, pipe longitudinal elasticity, and pipe distance off bottom. However, another factor that has not been included in either the steady-state or the unsteady-state models is the pipe eccentricity.

Because of the numerical nature of the model developed in this study, the application of the model to surge pressure calculations becomes rather simple. By simply changing the zero velocity boundary condition on the inner pipe to the velocity of the pipe, v_p , the velocity profiles and frictional pressure losses in concentric and eccentric annuli with inner pipe motion are calculated (Fig. 6.1). Thus, with this steady-state model, the effect of pipe eccentricity on surge pressures can be evaluated.

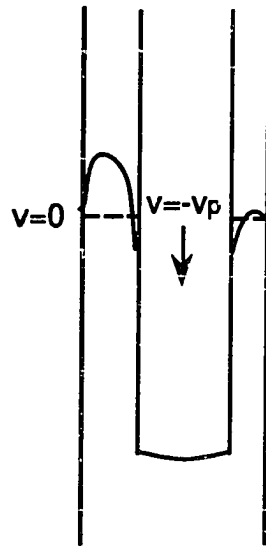


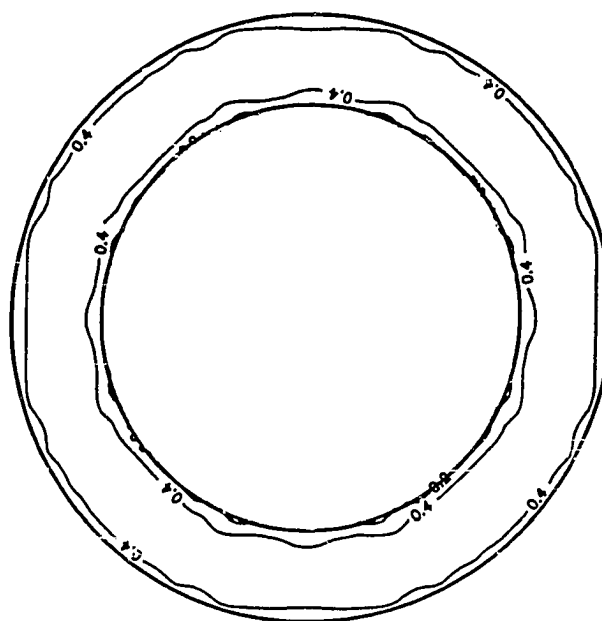
Fig. 6.1 Velocity profile in an eccentric annulus
while inner pipe is running into hole

6.1.1 Velocity Profiles and Frictional Pressure Loss Calculations with Inner Pipe Motion

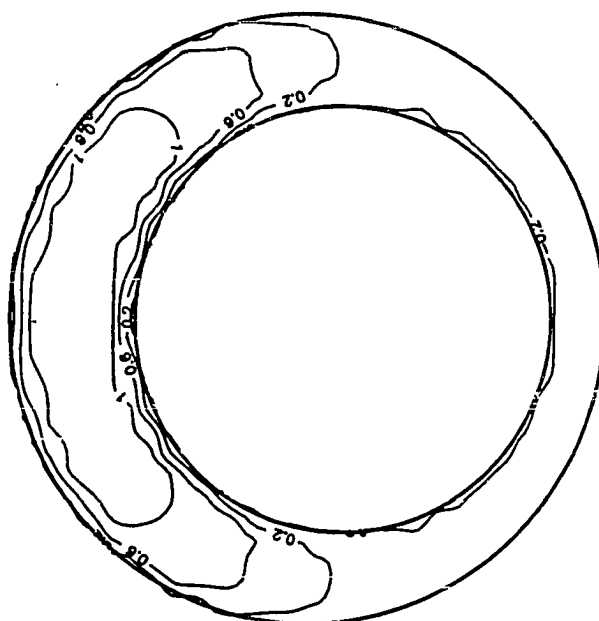
Let us assume that the Bingham plastic fluid ($\mu_p=25$ cp and $\tau_y=10$ lb/100ft²) used in the previous chapter is in a 10 in. diameter hole and a 7 in. casing string is being lowered. Then, the flow rate is equal to the rate of casing displacement:

$$Q = \frac{\pi}{4} d_i^2 v_p \quad (6.1)$$

where Q = flow rate, $L^3 T^{-1}$
 d_i = inner pipe diameter, L
 v_p = pipe velocity, $L T^{-1}$

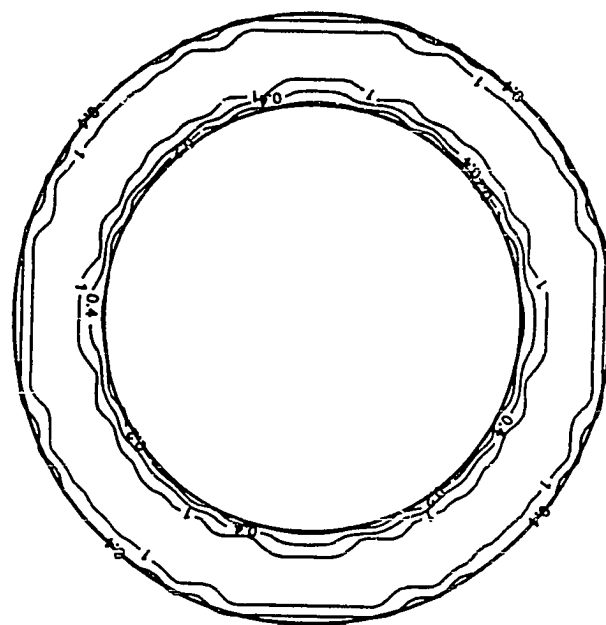


(a)

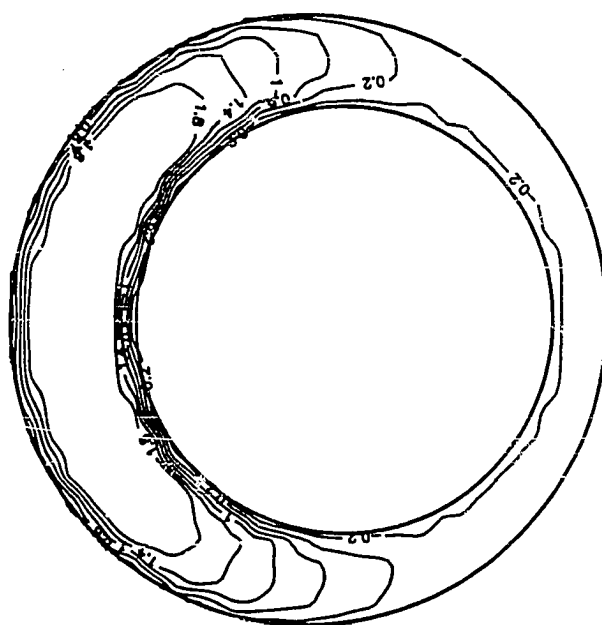


(b)

Fig. 6.2 Velocity profile while inner pipe is moving at 0.5 ft/s:
(a) concentric annulus, $e=0$, (b) eccentric annulus, $e=0.4$



(a)



(b)

Fig. 6.3 Velocity profile while inner pipe is moving at 1.0 ft/s:
(a) concentric annulus, $e=0$, (b) eccentric annulus, $e=0.4$

Figures 6.2 and 6.3 show the velocity profiles predicted by the model at concentric and eccentric annulus while the casing string is lowered at two different speeds. As can be seen, the pattern of the velocity profiles are quite similar to velocity profiles with no pipe motion (Figs. 5.8b and 5.9b). Even at relatively high casing lowering speeds ($v_p=1$ ft/s), the region of negative flow (the fluid clinging and flowing in the same direction as the casing) is extremely small. In the eccentric case, the region of negative flow slightly enlarges in the narrow part of the annulus because there is no positive flow to push it closer to the inner pipe. These types of velocity profiles can be utilized in the modelling of casing reciprocation as well. For surge pressure calculations, the frictional pressure loss is needed. Table 6.1 presents the change in frictional pressure loss with varying eccentricity for the above fluid.

Table 6.1 Frictional pressure loss gradient data of the Bingham plastic fluid with inner pipe motion

e (d'less)	$v_p = 0.5$ ft/s		$v_p = 1.0$ ft/s	
	$\Delta P_f / \Delta L$ (psi/ft)	R (d'less)	$\Delta P_f / \Delta L$ (psi/ft)	R (d'less)
0.00	0.01590	1.00	0.01850	1.00
0.40	0.01346	0.85	0.01560	0.84
0.80	0.01047	0.66	0.01182	0.64

This example shows a decrease of approximately 35% for the

frictional pressure loss gradient for an eccentricity of 0.8 relative to concentric pipe. For fluids with a yield point (Yield-Power law or Bingham plastic), the ratio of frictional pressure losses calculated in eccentric annulus to concentric annulus, R , is a weak function of pipe velocity, v_p . However, in case of Power law fluids, R remains independent of v_p as long as the flow is laminar. Therefore, the correlation developed (Eq. 5.8) in Chapter V is valid for surge pressure calculations also:

$$R = 1 - 0.072 \frac{e}{n} \left(\frac{d_i}{d_o} \right)^{0.8454} - 1.5 e^2 \sqrt{n} \left(\frac{d_i}{d_o} \right)^{0.1852} + 0.96 e^3 \sqrt{n} \left(\frac{d_i}{d_o} \right)^{0.2527} \quad (6.2)$$

The existing surge pressure models can be extended to include pipe eccentricity by simply incorporating R into these models.

6.1.2 An Example Calculation

In a directional well, a 7 in. casing string is being lowered at a speed of 0.5 ft/s into a 10 in. hole. The diameter of casing centralizers is 8.5 in. and the mud in the hole has a flow behavior index, n , of 0.8 and a consistency index, K , of 300 eq. cp. With a conventional concentric annular surge model, a frictional pressure loss gradient, $\Delta P_f / \Delta L$, of 0.0122 psi/ft is predicted. Assuming the centralizers touching the low-side-of-the-hole, the eccentricity from Eq. 1.2 is

$$e = \frac{d_o - d_c}{d_o - d_i} = \frac{10 - 8.5}{10 - 7} = 0.5 \quad (6.3)$$

Using Eq. 6.2, R is calculated;

$$R = 1 - 0.033 - 0.314 + 0.098 = 0.751$$

then, the frictional pressure loss gradient in the directional section of the well is

$$\left(\frac{\Delta P_f}{\Delta L}\right)_e = \left(\frac{\Delta P_f}{\Delta L}\right)_c R = 0.0122 \times 0.751 = 0.0092 \text{ psi/ft}$$

Figs. 5.13-5.16 show change in R as a function of e, n, and d_i/d_o . For typical drilling fluids, surge pressure calculation using concentric models may be very conservative (up to 100%) in directional wells.

6.2 Displacement of a Gas Kick in Solution in an Oil-Base Mud

When a gas kick is taken while circulating with an oil-base mud, high bottom hole pressures cause gas to go into solution in the liquid oil-base mud. In such cases, by the time a pit gain is detected, dangerously high volumes of gas may enter the well (when gas goes into solution the pit gain is slow since the mud expansion is small). As the mud is circulated out through a controlling choke, the pressures will decrease to a value below bubble point at some depth in the well causing gas to leave the solution. Therefore, the released gas displaces large volumes of mud from the hole, and decreases the bottom hole pressures to lower levels. After detection, the kick must be circulated out of

the well through an adjustable choke at the surface while keeping the bottom hole pressure constant and slightly above the formation pressure. To achieve this, a knowledge of the location of the kick is needed such that an accurate pressure profile can be predicted.

Here a prototype kick displacement model is developed, accounting for the velocity profiles in an annulus. It is assumed that all the gas entering the well goes into solution. The gas contaminated region of the oil-base mud is assumed to have the same viscous properties as the uncontaminated region and the single phase velocity profiles can be used. It is also assumed that the gas enters the hole as slug whereupon the well is shut-in to prevent further entry. Consequently, its shape will deform as a function of the fluid velocity profile as it is displaced. The model calculates the fraction of annulus occupied by gas contaminated mud, f_A , as a function of depth (Fig. 6.4). Also, by integrating the individual flow rates of each grid, the flow rate of gas contaminated mud as a function of time at a given depth can be calculated. Since most conventional kick models assume that the kick travels at an average velocity, a more realistic kick profile with displacement is obtained with this approach. Once again, the velocity profiles predicted by the eccentric model can be used to track the displacement of a gas kick in an oil-base mud as long as it remains in solution. Once the gas bubbles come out of the liquid phase, the model would have to be modified so it could account for gas expansion, bubble rise velocity or slip

velocity. The question of gas bubble rise and slip velocity has been investigated by others (Casariego, 1987) and it is not the intention of this work to address these difficulties.

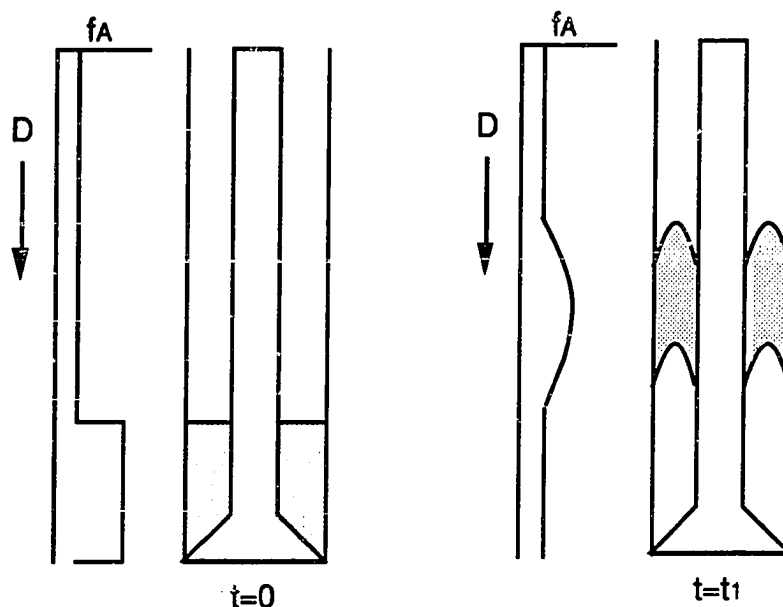


Fig. 6.4 A schematic of kick profiling

6.2.1 An Example Case

A 4.5" OD drillstring is in a 10 in. diameter hole, 6000 ft deep. While it is being drilled with an oil-base mud ($n=0.7$ and $K=300$ eq. cp), a gas kick is taken. The kick goes into solution and contaminates 30 bbl of mud. The gas contaminated mud is circulated out at 150 gpm while an adjustable choke is used at the surface. Assuming that the choke pressure is high enough to keep the gas in solution, and ignoring the expansion of the oil-

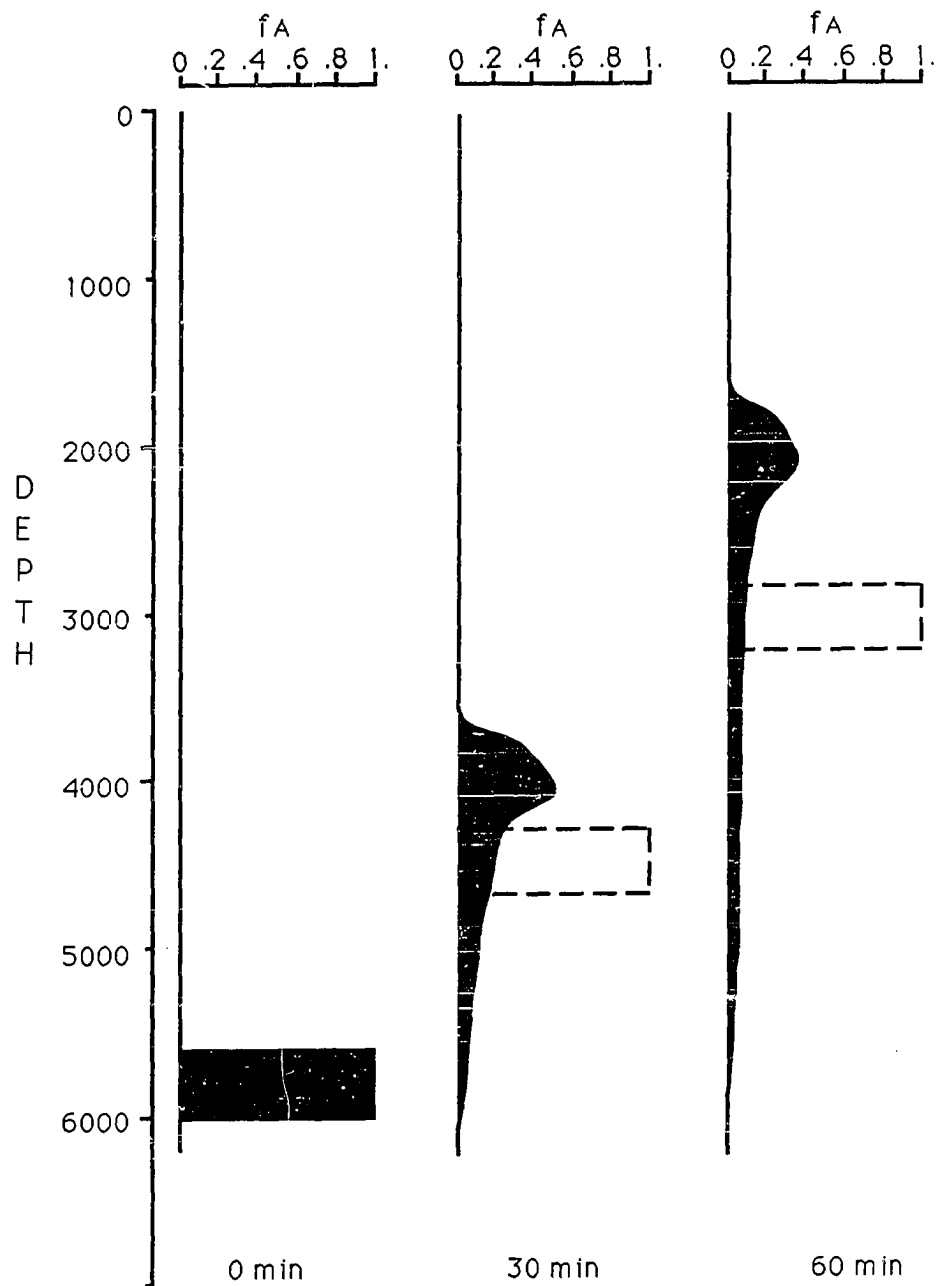


Fig. 6.5 Kick profile in concentric annulus, $e=0$

base mud as it approaches the surface (constant density), the model tracks the location of the kick. Fig. 6.5 shows the areal fraction of gas contaminated regions during the displacement assuming the annulus is concentric. The kick is at the bottom of the hole as a slug at time zero. Later, as displacement occurs, the kick begins to smear (fractions less than 1). After 30 and 60 min. of displacement, a high concentration leading edge is observed. The dashed lines show the location of the kick if the kick is assumed to be moving at the average velocity. Notice that the fraction is always one in that case. The flow rate of contaminated mud at the surface is shown in Fig. 6.6. If the volume of gas dissolved in oil is known, then the gas contaminated mud flow rate could be converted to a gas flow rate.

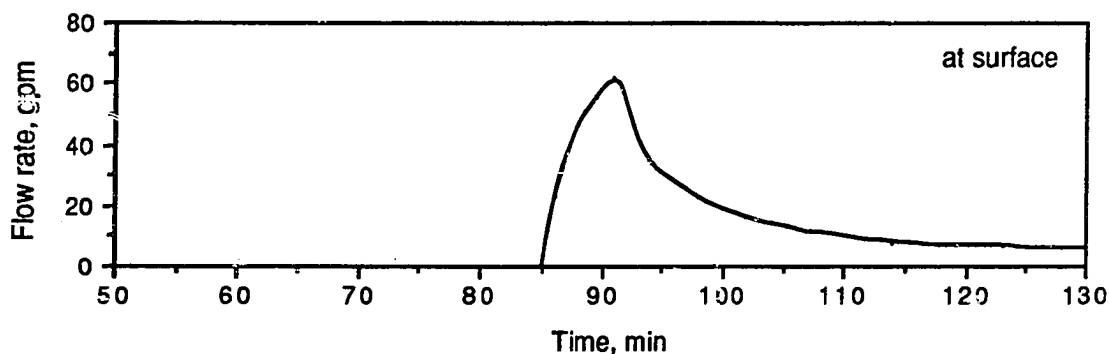


Fig. 6.6 Flow rate of contaminated oil-base mud at the surface, $e=0$

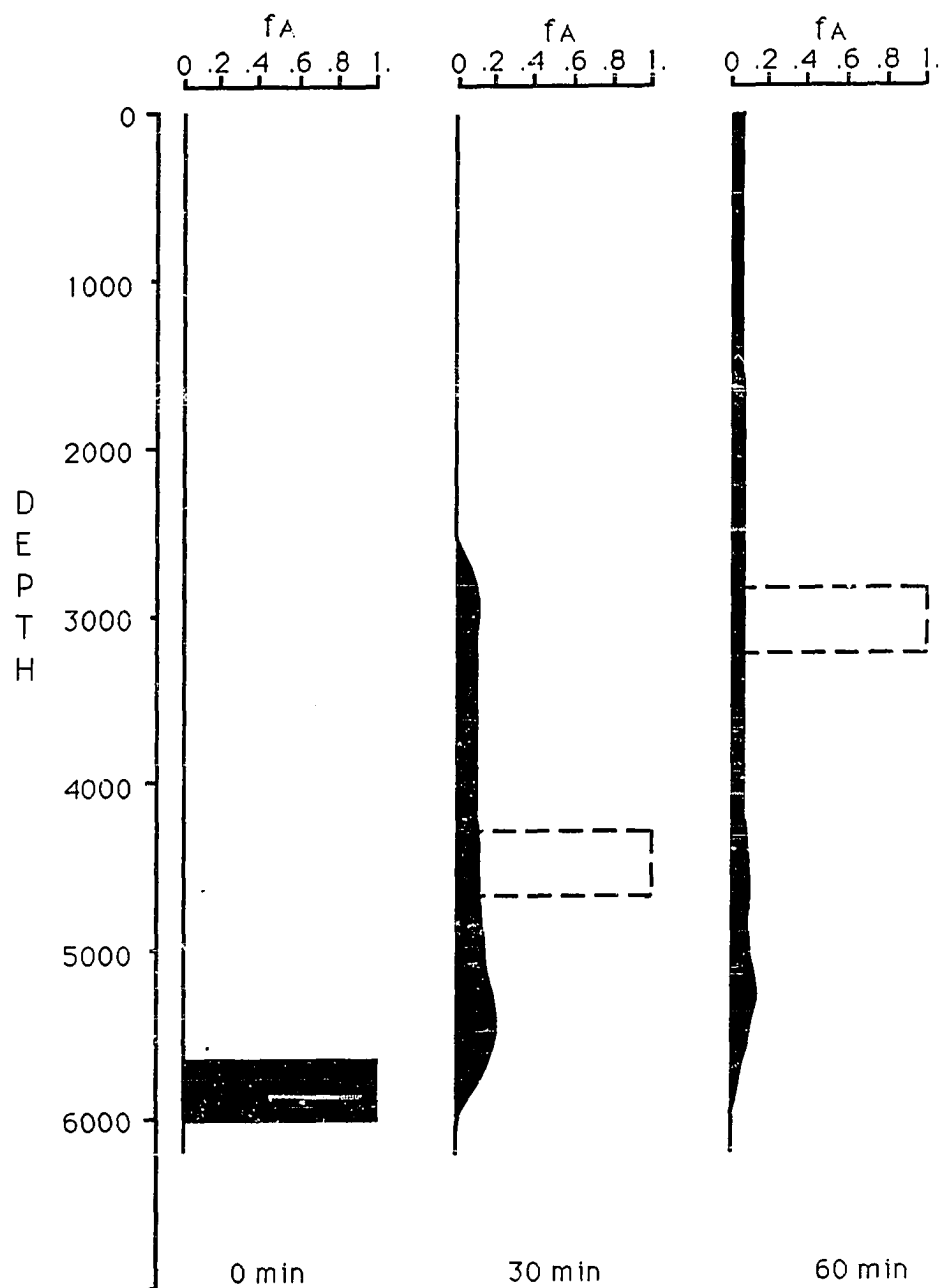


Fig. 6.7 Kick profile in eccentric annulus, $e=0.5$

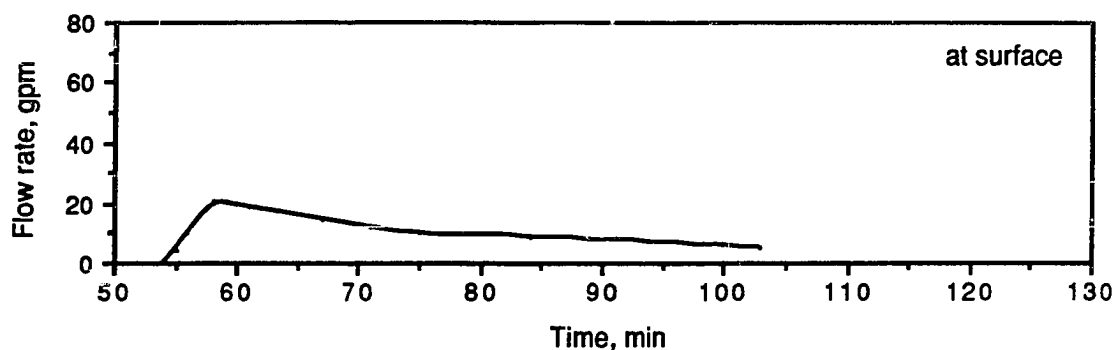


Fig. 6.8 Flow rate of contaminated oil-base mud at the surface, $e=0.5$

For an eccentricity of 0.5, the predicted kick profiles are longer and; therefore, less concentrated (Fig. 6.7) The strong smearing is the expected outcome of the velocity profiles in an eccentric annulus. The first gas show at the surface, in this case, is much earlier and flow rates are lower (Fig. 6.8).

In this study, the eccentricity and viscous properties of the mud have found to be important parameters in calculating arrival time of a kick and the degree of kick smearing.

CHAPTER VII

CONCLUSIONS AND RECOMMENDATIONS

7.1 Conclusions

1. The previous studies of eccentric annular flow with a slot flow approximation have been shown to employ an inadequate equation of motion.
2. The equation of motion has been derived with a new set of dimensionless groups that allows the evaluation of constant flow rate cases. Also, complex Yield-Power law (Herschel and Bulkley) rheological model has been incorporated into the equation of motion.
3. A rigorous numerical solution of the equation of motion has been developed to predict velocity profiles, viscosity profiles, and frictional pressure loss gradients in eccentric annuli.
4. The velocity profiles are substantially altered in the annulus when the inner pipe is no longer concentric. A high velocity region in the wide part of the annulus and a low velocity region (sometimes stagnant) in the narrow part of the annulus are calculated.

5. The average velocities have been found to be far from representative of the velocity profile in eccentric annuli.
6. The viscosity profiles generated for non-Newtonian fluids have shown that extremely high viscosity regions exist in most of the flow area, implying very little or no shear at all, and low viscosity regions near the pipe walls if a steep velocity profile exists.
7. Therefore, non-Newtonian fluids have been shown to flow over a long range of shear stress-shear rate curve at a given flow rate.
8. Apparent viscosities calculated near the pipe walls have been shown to be much lower than the overall viscosity profile revealed in the flow area.
9. The eccentricity is an important factor in calculating frictional pressure losses. In most cases, a 50% reduction in frictional pressure loss gradient is realized when inner pipe is fully eccentric, as compared to concentric annular flow at the same flow rate.
10. A correlation has been developed from the model generated data to calculate frictional pressure losses of Power law

fluids in eccentric annuli.

11. The model has been extended to surge pressure calculations by allowing inner pipe movement. The velocity profiles and frictional pressure loss gradients in concentric and eccentric annuli are calculated. The correlation developed for Power law fluids has been found to be valid in this case as well.
12. A simple technique of kick tracking in oil-base muds has been presented.

7.2 Recommendations

1. The extremely low shear rate region (0.001 to 1 sec^{-1}) for typical drilling fluids should be investigated experimentally.
2. The study raises questions on the validity of the concept of an average velocity in an eccentric annulus and the apparent viscosity of non-Newtonian fluids in general. A theoretical work should be conducted to modify or replace the average velocity and the apparent viscosity concepts.
3. The applications shown here should be extended to full models, and effects of eccentricity on other problems need to be investigated.

REFERENCES

Bird, R., Stewart, W.E., and Lightfoot, E.N.: *Transport Phenomena*, John & Sons, 1960, pp. 102-103.

Bourgoyne, A.T., Jr., Milhelm, K.K., Chenevert, M.E., and Young, F.S.: *Applied Drilling Engineering*, SPE Textbook Series, Vol. 2, 1986, pp. 104.

Burkhardt, J.A.: "Wellbore Pressure Surges Produced by Pipe Movement," JPT, June 1961, pp. 595-605.

Casariego, V.: "Generation, Migration, and Transportation of Gas Contaminated Regions of Drilling Fluid," Ph.D. Dissertation, LSU, 1987.

Denis, J.H., and Guillot, D.J.: "Prediction of Cement Slurry Laminar Pressure Drops by Rotational Viscometer," SPE/IADC 16137, presented at SPE/IADC Drilling Conf., New Orleans, LA, 1987, pp. 755-762.

Dodge, N.A.: "Friction Losses in Annular Flow," Paper Number 63-WA-11, presented at the Winter Annual Meeting of the ASME, Philadelphia, Pa, Nov. 17-22, 1963, pp. 1-7.

Fontenot, J.E., and Clark, R.K.: "An Improved Method for Calculating Swab and Surge Pressures and Circulating Pressures in a Drilling Well," SPEJ, Oct. 1974, pp. 451-462.

Fredrickson, A.G., and Bird, R.B.: "Non-Newtonian Flow in Annuli," Ind. and Chem. Eng., Vol. 50, March 1958, pp. 347-352.

Guckes, T.L.: "Laminar Flow of Non-Newtonian Fluids in an Eccentric Annulus," Trans. ASME, Vol. 97, Part 1, May 1975, pp. 498-506.

Herschel, W.H., and Bulkley, R.: "Measurement of Consistency as Applied to Rubber-Benzene Solutions," Proc. Am. Soc. Test. Mat., Vol. 26, 1926, pp. 621-633.

Heyda, J.F.: "A Green's Function Solution for the Case of Laminar Incompressible Flow Between Non-Concentric Circular Cylinders," J. Franklin Inst., Vol. 267, Jan. 1959, pp. 25-34.

Imco Services: *Applied Mud Technology*, Chapter 6, Seventh ed., 1983, pp. 6.

Iyoho, A.W., and Azar, J.J.: "An Accurate Slot-Flow Model for Non-Newtonian Fluid Flow Through Eccentric Annuli," SPEJ., Vol. 21, Oct. 1981, pp. 565-572.

Jonsson, V.K., and Sparrow, E.M.: "Experiments on Turbulent Flow Phenomena in Eccentric Annular Ducts," *Journal of Fluid Mechanics*, Vol. 25, part 1, 1966, pp. 65-86.

Lal, M.: "Surge and Swab Modeling for Dynamic Pressures and Safe Trip Velocities," IADC/SPE 11412, presented at the 1983 Drilling Conference, Dallas, TX, Feb. 20-23, 1983, pp. 427-433.

Lamb, H.: *Hydrodynamics*, sixth ed., Dover Publications, New York, 1945, pp. 585-587.

Lubinski, A., Hsu, F.H., and Nolte, K.G.: "Transient Pressure Surges Due to Pipe Movement in an Oil Well," *Revue de l'Inst. Franc. du Pet.*, May-June 1977, pp. 307-347.

Luo, Y., and Peden, J.M.: "Flow of Drilling Fluids Through Eccentric Annuli," SPE 16692, presented at 62nd Annual Tech. Conf. of SPE, Dallas, TX, Sept. 27-30, 1987, pp. 389- 396.

Mitchell, R.F.: "Dynamic Surge/Swab Pressure Predictions," SPE Drilling Engineering, Sept. 1988a, pp. 325-333.

Mitchell, R.F.: "Surge Pressure: Are Steady-State Models Adequate?" SPE 18021, presented at the 63rd Annual Technical Conference of SPE, Houston, TX, Oct. 2-5, 1988b, pp. 29-38.

Mitsuishi, N., and Aoyagi, Y.: "Non-Newtonian Fluid Flow in an Eccentric Annulus," J. Chem. Eng. Japan, Vol. 6, 1973, pp. 402-408.

Patankar, S.V.: *Numerical Heat Transfer and Fluid Flow*, McGraw-Hill Book Co., 1983, pp. 25-78.

Redberger, P.J., and Charles, M.E.: "Axial Laminar Flow in a Circular Pipe Containing a Fixed Core," Can. J. Chem. Eng., Vol. 40, August 1962, pp. 148-151.

Shuch, F.J.: "Computer Makes Surge-Pressure Calculations Useful," Oil and Gas Journal, August 3, 1964, pp. 96-104.

Snyder, W.T., and Goldstein, G.A.: "An Analysis of Fully Developed Laminar Flow in an Eccentric Annulus," Am. Inst. Chem. Eng. J., Vol. 11, 1965, pp. 462-467.

Spiegel, M.R.: *Mathematical Handbook of Formulas and Tables*, McGraw-Hill Book Co., 1968, pp. 125-128.

Tao, L.N., and Donovan, W.F.: "Through-Flow in Concentric and Eccentric Annuli of Fine Clearance With and Without Relative Motion of the Boundaries," Trans. ASME, Vol. 77, Nov. 1955, pp. 1291-1299.

Uner, D., Ozgen, C., and Tosun, I.: "Flow of a Power- Law Fluid in an Eccentric Annulus," SPE Drilling Engineering, Sept. 1989, pp.

269-272.

Vaughn, R.D.: "Axial Laminar Flow of Non-Newtonian Fluids in Narrow Eccentric Annuli," SPEJ, Vol. 5, Dec. 1965, pp. 277-280.

Welty, J.R., Wicks, C.E., and Wilson, R.E.: *Fundamentals of Momentum Heat and Mass Transfer*, third ed., John Wiley & Sons, 1984, pp. 107.

Zamora, M., and Lord, D.L.: "Practical Analysis of Drilling Mud Flow in Pipes and Annuli," SPE 4976, presented at 49th Fall Meeting of SPE, Houston, TX, 1974, pp. 1-16.

APPENDIX A

TRANSFORMATION OF THE EQUATION OF MOTION TO BIPOLAR COORDINATES

The equation of Motion in the cartesian coordinate system is:

$$\frac{\Delta P_f}{\Delta L} + \frac{\partial}{\partial x} \left(\mu \frac{\partial v}{\partial x} \right) + \frac{\partial}{\partial y} \left(\mu \frac{\partial v}{\partial y} \right) = 0 \quad (\text{A.1})$$

The transformed equation in bipolar coordinates should look like (Spiegel, 1968):

$$\frac{\Delta P_f}{\Delta L} + \frac{1}{h_1 h_2} \left[\frac{\partial}{\partial \epsilon} \left(\frac{h_2}{h_1} \mu \frac{\partial v}{\partial \epsilon} \right) + \frac{\partial}{\partial \eta} \left(\frac{h_1}{h_2} \mu \frac{\partial v}{\partial \eta} \right) \right] = 0 \quad (\text{A.2})$$

where

$$h_1 = \left(\frac{\partial x}{\partial \epsilon} \right)^2 + \left(\frac{\partial y}{\partial \epsilon} \right)^2 \quad (\text{A.3})$$

$$h_2 = \left(\frac{\partial x}{\partial \eta} \right)^2 + \left(\frac{\partial y}{\partial \eta} \right)^2 \quad (\text{A.4})$$

The relationship between the cartesian and bipolar coordinates are defined by:

$$x = \frac{a \sinh \epsilon}{\cosh \epsilon - \cos \eta} \quad (\text{A.5})$$

$$y = \frac{a \sin \eta}{\cosh \epsilon - \cos \eta} \quad (\text{A.6})$$

Now, taking the derivatives of Eqs. A.5 and 6, the coefficients h_1 and h_2 can be evaluated.

$$\frac{\partial x}{\partial \epsilon} = \frac{a (1 - \cosh \epsilon \cdot \cos \eta)}{(\cosh \epsilon - \cos \eta)^2} \quad (\text{A.7})$$

$$\frac{\partial y}{\partial \epsilon} = \frac{-a \sinh \epsilon \cdot \sin \eta}{(\cosh \epsilon - \cos \eta)^2} \quad (\text{A.8})$$

$$\frac{\partial y}{\partial \eta} = \frac{a (\cosh \epsilon \cdot \cos \eta - 1)}{(\cosh \epsilon - \cos \eta)^2} \quad (\text{A.9})$$

$$\frac{\partial x}{\partial \eta} = \frac{-a \sinh \epsilon \cdot \sin \eta}{(\cosh \epsilon - \cos \eta)^2} \quad (\text{A.10})$$

Substituting Eqs. A.7 and A.8 into Eq. A.3, and simplifying, we get:

$$h_1 = \frac{a}{\cosh \epsilon - \cos \eta} \quad (\text{A.11})$$

Similar treatment of Eq. A.4 yields:

$$h_2 = \frac{a}{\cosh \epsilon - \cos \eta} \quad (\text{A.12})$$

We observe that $h_1=h_2$ which simplifies the Eq. A.2. Substituting the values of h_1 and h_2 into Eq. A.2 and rearranging the terms, we have the equation of motion in bipolar coordinates.

$$\left(\frac{a}{\cosh \varepsilon - \cos \eta}\right)^2 \frac{\Delta P_f}{\Delta L} + \frac{\partial}{\partial \varepsilon} \left(\mu \frac{\partial v}{\partial \varepsilon} \right) + \frac{\partial}{\partial \eta} \left(\mu \frac{\partial v}{\partial \eta} \right) = 0 \quad (\text{A.13})$$

APPENDIX B

DERIVATION OF THE DIMENSIONLESS EQUATION OF MOTION

The equation of motion (3.22) in bipolar coordinates is expressed as:

$$\left(\frac{a}{\psi}\right)^2 \frac{\Delta P_f}{\Delta L} + \frac{\partial}{\partial \varepsilon} \left(\mu \frac{\partial v}{\partial \varepsilon} \right) + \frac{\partial}{\partial \eta} \left(\mu \frac{\partial v}{\partial \eta} \right) = 0 \quad (\text{B.1})$$

$$\text{also} \quad a = r_i \sinh \varepsilon_i = r_o \sinh \varepsilon_o \quad (\text{B.2})$$

$$\psi = \cosh \varepsilon - \cos \eta \quad (\varepsilon_o \leq \varepsilon \leq \varepsilon_i, \quad 0 \leq \eta \leq 2\pi) \quad (\text{B.3})$$

where $\frac{\Delta P_f}{\Delta L}$ = frictional pressure loss gradient, $M L^{-2} T^{-2}$
 μ = viscosity, $M L^{-1} T^{-1}$
 v = velocity, $L T^{-1}$
 r_o = radius of inner pipe, L
 r_i = radius of outer pipe, L

for a Yield-Power law fluid, the viscosity term in above equation is given by Eqs. 3.28 and 3.30:

$$\mu = \frac{\tau_o}{\dot{\gamma}} + K \dot{\gamma}^{n-1} \quad (\text{B.4})$$

$$\gamma = \left| \frac{\psi}{a} \sqrt{\left(\frac{\partial v}{\partial \varepsilon} \right)^2 + \left(\frac{\partial v}{\partial \eta} \right)^2} \right| \quad (\text{B.5})$$

the dimensionless velocity and dimensionless frictional pressure loss gradient are defined by Eqs. 3.32 and 3.33 which can be rearranged as:

$$v = \left(\frac{K}{\rho r_o^2} \right)^{\frac{1}{2-n}} v_D \quad (\text{B.6})$$

$$\frac{\Delta P_f}{\Delta L} = \left(\frac{K^2}{\rho^n r_o^{n+2}} \right)^{\frac{1}{2-n}} f \quad (\text{B.7})$$

substituting Eq. B.6 into B.5, shear rate can be expressed in terms of dimensionless velocity:

$$\gamma = \left(\frac{K}{\rho r_o^2} \right)^{\frac{1}{2-n}} \frac{1}{\sinh \varepsilon_o} \gamma_D \quad (\text{B.8})$$

where dimensionless shear rate, γ_D , is defined as:

$$\gamma = \left| \psi \sqrt{\left(\frac{\partial v_D}{\partial \varepsilon} \right)^2 + \left(\frac{\partial v_D}{\partial \eta} \right)^2} \right| \quad (\text{B.9})$$

thus, the viscosity can be written as:

$$\mu = \left(\frac{K}{\rho^{n-1} r_o^{2n-2}} \right)^{\frac{1}{2-n}} \mu_D \quad (\text{B.10})$$

where dimensionless viscosity, μ_D , is defined as:

$$\mu_D = \frac{\tau_D}{\gamma_D} \sinh \epsilon_o + \left(\frac{\sinh \epsilon_o}{\gamma_D} \right)^{1-n} \quad (\text{B.11})$$

also by definition the dimensionless yield point is

$$\tau_D = \frac{\tau_o}{\left(\frac{K^2}{\rho^n r_o^{2n}} \right)^{\frac{1}{2-n}}} \quad (\text{B.12})$$

Now, combining these equations into Eq. B.1, The final form of the dimensionless equation of motion in bipolar coordinates is obtained:

$$\left(\frac{\sinh \epsilon_o}{\psi} \right)^2 f + \frac{\partial}{\partial \epsilon} \left(\mu_D \frac{\partial v_D}{\partial \epsilon} \right) + \frac{\partial}{\partial \eta} \left(\mu_D \frac{\partial v_D}{\partial \eta} \right) = 0 \quad (\text{B.13})$$

97

```

C
C CALCULATING THE BOUNDARIES OF THE PIPES IN BIPOLAR COORDINATES
C AND THE DIMENSIONS OF THE GRIDS
J1=NGRIDY+2
J2=J1-1
I1=NGRIDX+2
I2=I1-1
C
TOTAL=0.
TOTL(1)=0.
DO 24 J=1,NGRIDX
I=NGRIDX-J+1
X8=(I+1.)/I
X9=NGRIDX+1
DELX(J+1)=(DLOG(X8))*E/((DLOG(X9))*E*NGRIDX**((1-E))*3.1415927
24 TOTAL=TOTAL+DELX(J+1)
DO 23 J=1,NGRIDX
DELX(J+1)=DELX(J+1)*3.1415927/TOTAL
23 TOTL(J+1)=TOTL(J)+DELX(J+1)
DELX(1)=DELX(2)
DELX(I1)=DELX(I2)
C
XM=E*(D2-D1)/D2
X1=(1.-S*S-XM*XM)/2/S/XM
X2=(1.-S*S+XM*XM)/2/XM
EPS1=DLOG(X1+DSQRT(X1*X1-1))
EPS2=DLOG(X2+DSQRT(X2*X2-1))
DELY=(EPS1-EPS2)/NGRIDY
DSI=DSINH(EPS2)
C
C STARTING LINE-BY-LINE METHOD, SETTING THE COEFFICIENTS AT
C THE BOUNDARIES
DO 51 I=2,I2
A(I,1)=1.
B(I,1)=0.
C(I,1)=0.
D(I,1)=0.
P(I,1)=B(I,1)/A(I,1)
Q(I,1)=D(I,1)/A(I,1)
P(I,J1)=.
51 Q(I,J1)=.
C
C GUESSING A VELOCITY FIELD
DO 52 I=1,I1
DO 52 J=1,J1
V(I,J)=VGUESS
52 IF(J.EQ.1.OR.J.EQ.J1) V(I,J)=0.
WRITE(6,511) S,E,XN,XX,TAUD,DPDL,VISLIM,FCONST
S,QCONST,VCONST,VISCON,VGUESS*VCONST
511 FORMAT(/,3X,'DATA:',/,3X,'D1/D2=',F5.3,5X,'E=',F5.3,4X,'N=',
$F7.4,3X,'K=',F7.2,' EQ. CP',3X,'YIELD POINT=',F5.1,
$' LB/100 SQ. FT',/,3X,'DP/DL=',F10.8,' PSI/FT',2X,
$//,3X,'VISL=',E12.5,3X,'FCONST=',E12.5,3X,'QCONST=',E12.5
$,/,3X,'VCONST=',E12.5,3X,'VIS CONST=',E12.5,3X,'VAVG=',F6.3,'FT/S'
$//,3X,'FLOW RATE CALCULATIONS:')
C
C INITIALIZING FLOW RATE, PRINTING COUNTER, AND ITERATION COUNTER
QT1=0.
IPRINT=0
ITER=0
C

```

```

00380000
00590000
00600000
00610000
00620000
00630000
00640000
00650000
00660000
00670000
00680000
00690000
00700000
00710000
00720000
00730000
00740000
00750000
00760000
00770000
00780000
00790000
00800000
00810000
00820000
00830000
00840000
00850000
00860000
00870000
00880000
00890000
00900000
00910000
00920000
00930000
00940000
00950000
00960000
00970000
00980000
00990000
01000000
01010000
01020000
01030000
01040000
01050000
01060000
01070000
01080000
01090000
01100000
01110000
01120000
01130000
01140000
01150000
01160000
01170000
01180000

```



```

C   REPEATING TO OBTAIN AN "IMPROVED VELOCITY" FIELD          01190000
100 CONTINUE                                                    01200000
C   COMPUTING AN AVERAGE VELOCITY AT THE SOUTH-WEST CORNER OF  01210000
C   EACH CONTROL-VOLUME                                         01220000
DO 53 I=2,I1                                                    01230000
DO 53 J=2,J1                                                    01240000
53 V1(I,J)=.5*(DELX(I-1)*(V(I,J)+V(I,J-1))+DELX(I)*(V(I-1,J)+ 01250000
SV(I-1,J-1)))/(DELX(I)+DELX(I-1))                               01260000
C   CALCULATING VISCOSITY AT THE WEST FACE OF EACH CONTROL-VOLUME 01270000
C   DO 31 I=2,I1                                                01280000
DO 31 J=2,J2                                                    01290000
DVDX1=DABS(V(I,J)-V(I-1,J))/((DELX(I-1)+DELX(I))/2)           01300000
DVDY1=DABS(V1(I,J)-V1(I,J+1))/DELY                             01310000
IF(J.EQ.2.OR.J.EQ.J2) DVDY1=4*DVDY1/3                          01320000
C1=DVDX1*DVDX1+DVDY1*DVDY1                                       01330000
IF(C1.LT.VISLIM) C1=VISLIM                                       01340000
ETA=TOTL(I-1)                                                    01350000
EPS=EPS2+(J-2)*DELY+DELY/2.                                     01360000
XI=DCOSH(EPS)-DCOS(ETA)                                          01370000
SH1=XI*DSQRT(C1)                                                  01380000
VISB1(I,J)=TAUD*DSI/DABS(SH1)                                    01390000
IF(XN.LE.1.) VISP1(I,J)=DABS((DSI/SH1)**(1-XN))                01400000
IF(XN.GT.1.) VISP1(I,J)=DABS((SH1/DSI)**(XN-1))                01410000
31 VIS1(I,J)=VISP1(I,J)+VISB1(I,J)                               01420000
C   CALCULATING VISCOSITY AT THE SOUTH FACE OF EACH CONTROL-VOLUME 01430000
C   DO 32 I=2,I2                                                01440000
DO 32 J=2,J1                                                    01450000
DVDX2=DABS(V1(I,J)-V1(I+1,J))/DELX(I)                           01460000
DVDY2=DABS(V(I,J)-V(I,J-1))/DELY                                 01470000
IF(J.EQ.2.OR.J.EQ.J1) DVDY2=DVDY2*2.                            01480000
C2=DVDX2*DVDX2+DVDY2*DVDY2                                       01490000
IF(C2.LT.VISLIM) C2=VISLIM                                       01500000
ETA=TOTL(I-1)+DELX(I)/2                                          01510000
EPS=EPS2+(J-2)*DELY                                              01520000
IF(J.EQ.2) EPS=EPS+DELY/4.                                       01530000
IF(J.EQ.J1) EPS=EPS-DELY/4.                                       01540000
XI=DCOSH(EPS)-DCOS(ETA)                                          01550000
SH2=XI*DSQRT(C2)                                                  01560000
VISB2(I,J)=TAUD*DSI/DABS(SH2)                                    01570000
IF(XN.LE.1.) VISP2(I,J)=DABS((DSI/SH2)**(1-XN))                01580000
IF(XN.GT.1.) VISP2(I,J)=DABS((SH2/DSI)**(XN-1))                01590000
32 VIS2(I,J)=VISP2(I,J)+VISB2(I,J)                               01600000
C   COMPUTING THE COEFFICIENTS OF THE TDMA EQN.                01610000
C   DO 54 I=2,I2                                                01620000
DO 54 J=2,J2                                                    01630000
DELS=DELY                                                         01640000
DELN=DELY                                                         01650000
DELE=(DELX(I)+DELX(I+1))/2                                       01660000
DELN=(DELX(I)+DELX(I-1))/2                                       01670000
IF(J.EQ.2) DELS=DELY/2.                                          01680000
IF(J.EQ.J2) DELN=DELY/2.                                          01690000
DI=(DELE+DELN)/2.                                                01700000
DJ=(DELN+DELS)/2.                                                01710000
AN=VIS2(I,J+1)*DI/DELN                                           01720000
AS=VIS2(I,J)*DI/DELS                                             01730000
AE=VIS1(I+1,J)*DJ/DELE                                           01740000

```

```

      AW=VIS1(I,J)*DJ/DELW
      A(I,J)=AN+AS+AE+AW
      B(I,J)=AN
      C(I,J)=AS
      IF(I.EQ.2) V(I-1,J)=V(I,J)
      IF(I.EQ.I2) V(I+1,J)=V(I,J)
      ETA=TOTL(I-1)+DELX(I)/2.
      EPS=EPS2+(J-2)*DELY+DELY/2.
      XI=DCOSH(EPS)-DCOS(ETA)
      GARE(I,J)=DSI*DSI/XI/XI*DI*DJ
      D(I,J)=AE*V(I+1,J)+AW*V(I-1,J)+GARE(I,J)*F
      P(I,J)=B(I,J)/(A(I,J)-C(I,J)*P(I,J-1))
      Q(I,J)=(C(I,J)*Q(I,J-1)+D(I,J))/(A(I,J)-C(I,J)*P(I,J-1))
54  CONTINUE
C
C  CALCULATING "NEW" VELOCITY FIELD
      DO 55 I=2,I2
      DO 55 J=2,J2
      J=J2-N+2
55  VN(I,J)=P(I,J)*V(I,J+1)+Q(I,J)
      DO 555 I=2,I2
      DO 555 J=2,J2
555  V(I,J)=VN(I,J)
C
C  COUNTING NUMBER OF ITERATIONS
      IPRINT=IPRINT+1
      ITER=ITER+1
      IF(IPRINT.EQ.50) GO TO 500
      GO TO 100
500 CONTINUE
      IPRINT=0
      QT=0.
      VIST=0.
      AREA=0.
C
C  CALCULATING FLOW RATE
      DO 57 I=2,I2
      DO 57 J=2,J2
      AREA=AREA+GARE(I,J)
      FLORATE=V(I,J)*GARE(I,J)
57  QT=QT+FLORATE
      QT=2.*QT
      VAVG=QT/2/AREA
      WRITE(6,70) ITER,QT*QCONST,VAVG*VCONST,VISLIM
70  FORMAT(3X,'NO. ITER=',I4,3X,'FLOW RATE=',F8.1,' GPM',3X,
     & 'AVG. VELO=',F8.3,' FT/S',3X,'VISLIM=',E12.5)
      IF(DABS((QT1-QT)/QT).LT.CONLIM1) GOTO 444
      QT1=QT
C
C  LIMIT ON NUMBER OF ITERATIONS
      IF(ITER.LT.NITER) GO TO 100
      GO TO 445
444 VISLIM=VISLIM*1.D-2
      IF(VISLIM.LT.1.D-50) GO TO 445
      IF(DABS((QTVIS-QT)/QT).LT.CONLIM2) GOTO 445
      QTVIS=QT
      GO TO 100
445 CONTINUE
C
C  PRINTING VELOCITY FIELD
      IF(NVELO.NE.1) GO TO 800

```

```

01300000
01810000
01820000
01830000
01840000
01850000
01860000
01870000
01880000
01890000
01900000
01910000
01920000
01930000
01940000
01950000
01960000
01970000
01980000
01990000
02000000
02010000
02020000
02030000
02040000
02050000
02060000
02070000
02080000
02090000
02100000
02110000
02120000
02130000
02140000
02150000
02160000
02170000
02180000
02190000
02200000
02210000
02220000
02230000
02240000
02250000
02260000
02270000
02280000
02290000
02300000
02310000
02320000
02330000
02340000
02350000
02360000
02370000
02380000
02390000
02400000

```

DO 51 J=1,J1	02410000
DO 61 I=1,I1	02420000
61 V(I,J)=VCONST*V(I,J)	02430000
JM=J1/2	02440000
VMAX=V(2,JM)	02450000
CALL POWER(VMAX,IPOWER,POWR)	02460000
WRITE(6,71) IPCWR	02470000
71 FORMAT(/,3X,'VELOCITY PROFILE: (FT/S)',/,3X,'MULTIPLY BY E',I2)	02480000
DO 56 N=1,J1	02490000
J=J1-N+1	02500000
WRITE(6,510) (V(I,J)/PCWR,I=2,I2)	02510000
510 FORMAT(/,2X,20(F5.4,1X))	02520000
56 CONTINUE	02530000
300 CONTINUE	02540000
C	02550000
C PRINTING VISCOSITY FIELD	02560000
IF(MVISC.NE.1) GO TO 801	02570000
WRITE(6,72)	02580000
72 FORMAT('1',3X,'VISCOSITY PROFILE: (CP)',/,)	02590000
DO 89 N=2,J2	02600000
J=J2-N+2	02610000
WRITE(6,122) ((VIS2(I,J)+VIS2(I,J+1))*VISCON/2,I=2,I2)	02620000
122 FORMAT(/,3X,20(F5.0,1X))	02630000
89 CONTINUE	02640000
801 CONTINUE	02650000
STOP	02660000
END	02670000
C	02680000
C	02690000
SUBROUTINE POWER(XMAX,IPOWER,POWR)	02700000
IMPLICIT REAL*8 (A-H,O-Z)	02710000
IPOWER=0	02720000
POWR=1.	02730000
90 IF(XMAX.GT..09999) GO TO 91	02740000
XMAX=10*XMAX	02750000
IPOWER=IPOWER+1	02760000
POWR=POWR*.1	02770000
GO TO 90	02780000
91 IF(XMAX.LT.1.) GO TO 92	02790000
XMAX=.1*XMAX	02800000
IPOWER=IPOWER+1	02810000
POWR=POWR/.1	02820000
GO TO 91	02830000
92 CONTINUE	02840000
RETURN	02850000
END	02860000

VITA

Mustafa Hacıislamoglu, born on August 10, 1960 in Findikli, Rize, Turkey, is the eldest of three children of Yilmaz and Guzide Hacıislamoglu. He graduated from Haydarpasa High School in Istanbul, Turkey in June 1977, and enrolled at the Istanbul Technical University. Upon receiving a Bachelor of Science in Petroleum Engineering in June 1982, he was awarded a scholarship from the Department of Education of Turkey to pursue graduate studies in the U.S.A. He entered the graduate school in January 1984 at Louisiana State University, Baton Rouge, LA from which he received a Master's Degree in Petroleum Engineering in December 1985.

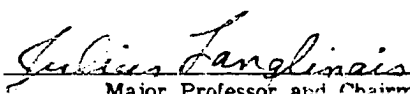
DOCTORAL EXAMINATION AND DISSERTATION REPORT


Candidate: Mustafa Hacıislamoglu

Major Field: Petroleum Engineering

Title of Dissertation: Non-Newtonian Fluid Flow In Eccentric Annuli And Its Application To Petroleum Engineering Problems

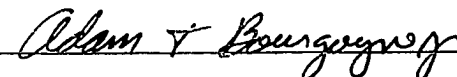
Approved:



Major Professor and Chairman

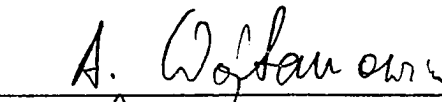

Dean of the Graduate School

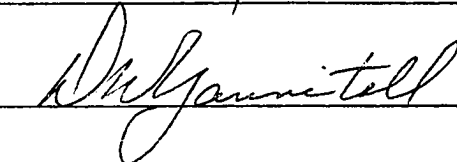
EXAMINING COMMITTEE:











Date of Examination:

December 4, 1989